

# Fundamental limits on the rate of bacterial cell division

<sup>3</sup> **Nathan M. Belliveau<sup>†, 1</sup>, Griffin Chure<sup>†, 2, 3</sup>, Christina L. Hueschen<sup>4</sup>, Hernan G.  
<sup>4</sup> Garcia<sup>5</sup>, Jané Kondev<sup>6</sup>, Daniel S. Fisher<sup>7</sup>, Julie Theriot<sup>1, 8</sup>, Rob Phillips<sup>2, 9, \*</sup>**

\*For correspondence:

<sup>†</sup>These authors contributed equally to this work

<sup>5</sup> <sup>1</sup>Department of Biology, University of Washington, Seattle, WA, USA; <sup>2</sup>Division of  
<sup>6</sup> Biology and Biological Engineering, California Institute of Technology, Pasadena, CA,  
<sup>7</sup> USA; <sup>3</sup>Department of Applied Physics, California Institute of Technology, Pasadena, CA,  
<sup>8</sup> USA; <sup>4</sup>Department of Chemical Engineering, Stanford University, Stanford, CA, USA;  
<sup>9</sup> <sup>5</sup>Department of Molecular Cell Biology and Department of Physics, University of  
<sup>10</sup> California Berkeley, Berkeley, CA, USA; <sup>6</sup>Department of Physics, Brandeis University,  
<sup>11</sup> Waltham, MA, USA; <sup>7</sup>Department of Applied Physics, Stanford University, Stanford, CA,  
<sup>12</sup> USA; <sup>8</sup>Allen Institute for Cell Science, Seattle, WA, USA; <sup>9</sup>Department of Physics,  
<sup>13</sup> California Institute of Technology, Pasadena, CA, USA; \*Contributed equally

<sup>14</sup> 

---

<sup>15</sup> **Abstract** This will be written next (promise).

<sup>16</sup> 

---

## <sup>17</sup> Introduction

<sup>18</sup> The range of bacterial growth rates is enormously diverse. In natural environments, some micro-  
<sup>19</sup> bial organisms might double only once per year while in comfortable laboratory conditions, growth  
<sup>20</sup> can be rapid with several divisions per hour. This six order of magnitude difference illustrates the  
<sup>21</sup> intimate relationship between environmental conditions and the rates at which cells convert nu-  
<sup>22</sup> trients into new cellular material – a relationship that has remained a major topic of inquiry in  
<sup>23</sup> bacterial physiology for over a century (*Jun et al., 2018*). As was noted by Jacques Monod, “the  
<sup>24</sup> study of the growth of bacterial cultures does not constitute a specialized subject or branch of re-  
<sup>25</sup> search, it is the basic method of Microbiology.” Those words ring as true today as they did when  
<sup>26</sup> they were written 70 years ago. Indeed, the study of bacterial growth has undergone a molecular  
<sup>27</sup> resurgence since many of the key questions addressed by the pioneering efforts in the middle of  
<sup>28</sup> the last century can be revisited by examining them through the lens of the increasingly refined  
<sup>29</sup> molecular census that is available for bacteria such as the microbial workhorse *Escherichia coli*. Sev-  
<sup>30</sup> eral of the outstanding questions that can now be studied about bacterial growth include: what  
<sup>31</sup> sets the fastest time scale that bacteria can divide, and how is growth rate tied to the quality of the  
<sup>32</sup> carbon source. In this paper, we address these two questions from two distinct angles. First, as  
<sup>33</sup> a result of an array of high-quality proteome-wide measurements of the *E. coli* proteome under a  
<sup>34</sup> myriad of different growth conditions, we have a census that allows us to explore how the num-  
<sup>35</sup> ber of key molecular players change as a function of growth rate. This census provides a window  
<sup>36</sup> onto whether the processes they mediate such as molecular transport into the cells and molecular  
<sup>37</sup> synthesis within cells can run faster. Second, because of our understanding of the molecular path-  
<sup>38</sup> ways responsible for many of the steps in bacterial growth, we can also make order of magnitude  
<sup>39</sup> estimates to infer the copy numbers that would be needed to achieve a given growth rate. In this  
<sup>40</sup> paper, we pass back and forth between the analysis of a variety of different proteomic datasets and  
<sup>41</sup> order-of-magnitude estimations to determine possible molecular bottlenecks that limit bacterial

42 growth and to see how the growth rate varies in different carbon sources.

43 Specifically, we leverage a combination of *E. coli* proteomic data sets collected over the past  
 44 decade using either mass spectrometry (*Schmidt et al., 2016; Peebo et al., 2015; Valgepea et al.,  
 45 2013*) or ribosomal profiling (*Li et al., 2014*) across 31 unique growth conditions. Broadly speaking,  
 46 we entertain several classes of hypotheses as are illustrated in **Figure 1**. First, we consider potential  
 47 limits on the transport of nutrients into the cell. We address this hypothesis by performing an  
 48 order-of-magnitude estimate for how many carbon, phosphorous, and sulfur atoms are needed to  
 49 facilitate this requirement given a 5000 second division time. As a second hypothesis, we consider  
 50 the possibility that there exists a fundamental limit on how quickly the cell can generate ATP. We  
 51 approach this hypothesis from two angles, considering how many ATP synthase complexes must  
 52 be needed to churn out enough ATP to power protein translation followed by an estimation of  
 53 how many electron transport complexes must be present to maintain the proton motive force.  
 54 A third class of estimates considers the need to maintain the size and shape of the cell through  
 55 the construction of new lipids for the cell membranes as well as the glycan polymers which make  
 56 up the rigid peptidoglycan. Our final class of hypotheses centers on the synthesis of a variety of  
 57 biomolecules. Our focus is primarily on the stages of the central dogma as we estimate the number  
 58 of protein complexes needed for DNA replication, transcription, and protein translation.

59 In broad terms, we find that the majority of these estimates are in close agreement with the  
 60 experimental observations, with protein copy numbers apparently well-tuned for the task of cell  
 61 doubling. This allows us to systematically scratch off the hypotheses diagrammed in **Figure 1** as  
 62 setting possible speed limits. Ultimately, we find that protein translation (particularly the genera-  
 63 tion of new ribosomes) acts as 1) a rate limiting step for the *fastest* bacterial division, and 2) the  
 64 major determinant of bacterial growth across all nutrient conditions we have considered under  
 65 steady state, exponential growth. This perspective is in line with the linear correlation observed  
 66 between growth rate and ribosomal content (typically quantified through the ratio of RNA to pro-  
 67 tein) for fast growing cells (*Scott et al., 2010*), but suggests a more prominent role for ribosomes  
 68 in setting the doubling time across all conditions of nutrient limitation. Here we again leverage the  
 69 quantitative nature of this data set and present a quantitative model of the relationship between  
 70 the fraction of the proteome devoted to ribosomes and the speed limit of translation, revealing  
 71 a fundamental tradeoff between the translation capacity of the ribosome pool and the maximal  
 72 growth rate.

### 73 Uptake of Nutrients

74 In order to build new cellular mass, the molecular and elemental building blocks must be scav-  
 75 enged from the environment in different forms. Carbon, for example, is acquired via the transport  
 76 of carbohydrates and sugar alcohols with some carbon sources receiving preferential treatment  
 77 in their consumption (*Monod, 1947*). Phosphorus, sulfur, and nitrogen, on the other hand, are har-  
 78 vested primarily in the forms of inorganic salts, namely phosphate, sulfate, and ammonia (*Jun et al.,  
 79 2018; Assentoft et al., 2016; Stasi et al., 2019; Antonenko et al., 1997; Rosenberg et al., 1977; Will-  
 80 sky et al., 1973*). All of these compounds have different permeabilities across the cell membrane  
 81 (*Phillips 2018*) and most require some energetic investment either via ATP hydrolysis or through  
 82 the proton electrochemical gradient to bring the material across the hydrophobic cell membrane.  
 83 Given the diversity of biological transport mechanisms and the vast number of inputs needed to  
 84 build a cell, we begin by considering transport of some of the most important cellular ingredients:  
 85 carbon, nitrogen, oxygen, hydrogen, phosphorus, and sulfur.

86 The elemental composition of *E. coli* has received much quantitative attention over the past  
 87 half century (*Neidhardt et al., 1991; Taymaz-Nikerel et al., 2010; Heldal et al., 1985; Bauer and  
 88 Ziv, 1976*), providing us with a starting point for estimating the copy numbers of various trans-  
 89 porters. While there is some variability in the exact elemental percentages (with different uncer-  
 90 tainties), we can estimate that the dry mass of a typical *E. coli* cell is  $\approx$  45% carbon (BNID: 100649,  
 91 *Milo et al. (2010)*),  $\approx$  15% nitrogen (BNID: 106666, *Milo et al. (2010)*),  $\approx$  3% phosphorus (BNID:

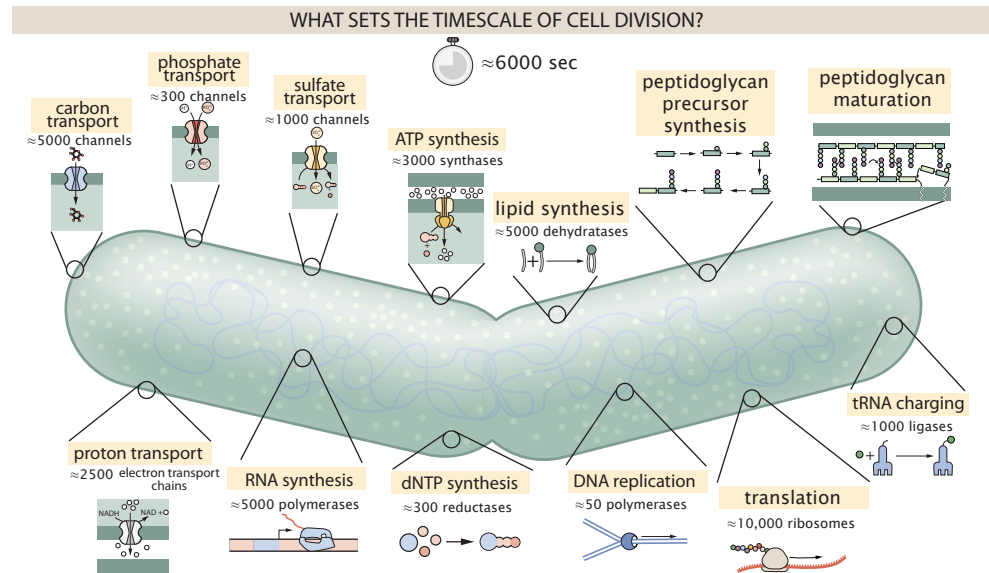


**Figure 1. Transport and synthesis processes necessary for cell division.** We consider an array of processes necessary for a cell to double its molecular components. Such processes include the transport of carbon across the cell membrane, the production of ATP, and fundamental processes of the central dogma namely RNA, DNA, and protein synthesis. A schematic of each synthetic or transport category is shown with an approximate measure of the complex abundance at a growth rate of 0.5 per hour. In this work, we consider a standard bacterial division time of  $\approx 5000$  sec.

92 100653, *Milo et al. (2010)*), and 1% sulfur (BNID: 100655, *Milo et al. (2010)*). In the coming para-  
 93 graphs, we will engage in a dialogue between back-of-the-envelope estimates for the numbers of  
 94 transporters needed to facilitate these chemical stoichiometries and the experimental proteomic  
 95 measurements of the biological reality. Such an approach provides the opportunity to test if our  
 96 biological knowledge is sufficient to understand the scale at which these complexes are produced.  
 97 Specifically, we will make these estimates considering a modest doubling time of 5000 s, a growth  
 98 rate of  $\approx 0.5 \text{ hr}^{-1}$ , the range in which the majority of the experimental measurements reside.

### 99 Nitrogen Transport

100 Before we begin our back-of-the-envelope estimations, we must address which elemental sources  
 101 must require proteinaceous transport, meaning that the cell cannot acquire appreciable amounts  
 102 simply via diffusion from the membrane. The permeability of the lipid membrane to a large num-  
 103 ber of solutes has been extensively characterized over the past century. Large, polar molecular  
 104 species (such as various sugar molecules, sulfate, and phosphate) have low permeabilities while  
 105 small, non-polar compounds (such as oxygen, carbon dioxide, and ammonia) can readily diffuse  
 106 across the membrane. Ammonia, a primary source of nitrogen in typical laboratory conditions,  
 107 has a permeability on par with water ( $\approx 10^5 \text{ nm/s}$ , BNID:110824 *Milo et al. (2010)*). In particularly  
 108 nitrogen-poor conditions, *E. coli* expresses a transporter (AmtB) which appears to aid in nitrogen  
 109 assimilation, though the mechanism and kinetic details of transport is still a matter of debate (*van*  
 110 *Heeswijk et al., 2013; Khademi et al., 2004*). Beyond ammonia, another plentiful source of nitrogen  
 111 come in the form of glutamate, which has its own complex metabolism and scavenging pathways.  
 112 However, nitrogen is plentiful in the growth conditions examined in this work, permitting us to ne-  
 113 glect nitrogen transport as a potential rate limiting process in cell division in typical experimental  
 114 conditions. We direct the reader to the supplemental information for a more in-depth discussion of  
 115 permeabilities and a series of calculations revealing that active nitrogen transport can be neglected  
 116 for the purposes of this article.

117 **Carbon Transport**

118 We begin our estimations with the most abundant element in *E. coli* by mass, carbon. Using  $\approx 0.3$   
 119 pg as the typical *E. coli* dry mass (BNID: 103904, *Milo et al. (2010)*), we estimate that  $\approx 10^{10}$  carbon  
 120 atoms must be brought into the cell in order to double all of the carbon-containing molecules (*Fig-*  
 121 *ure 2(A, top)*). Typical laboratory growth conditions, such as those explored in the aforementioned  
 122 proteomic data sets, provide carbon as a single class of sugar such as glucose, galactose, or xylose  
 123 to name a few. *E. coli* has evolved myriad mechanisms by which these sugars can be transported  
 124 across the cell membrane. One such mechanism of transport is via the PTS system which is a  
 125 highly modular system capable of transporting a diverse range of sugars (*Escalante et al., 2012*).  
 126 The glucose-specific component of this system transports  $\approx 200$  glucose molecules per second per  
 127 transporter (BNID: 114686, *Milo et al. (2010)*). Making the assumption that this is a typical sugar  
 128 transport rate, coupled with the need to transport  $10^{10}$  carbon atoms, we arrive at the conclusion  
 129 that on the order of 1,000 transporters must be expressed in order to bring in enough carbon  
 130 atoms to divide in 5000 s, diagrammed in the top panel of *Figure 2(A)*. This estimate, along with  
 131 the observed average number of the PTS system carbohydrate transporters present in the pro-  
 132 teomic data sets (*Schmidt et al., 2016; Peebo et al., 2015; Valgepea et al., 2013; Li et al., 2014*), is  
 133 shown in *Figure 2(A)*. While we estimate 1500 transporters are needed with a 5000 s division time,  
 134 we can abstract this calculation to consider any particular growth rate given knowledge of the cell  
 135 density and volume as a function of growth rate and direct the reader to the SI for more informa-  
 136 tion. As revealed in *Figure 2(A)*, experimental measurements exceed the estimate by several fold,  
 137 illustrating that transport of carbon in to the cell is not rate limiting for cell division. Abstracting  
 138 this point estimate at 5000 s to a continuum of growth rates (grey line in *Figure 2(A)*) reveals an  
 139 excess of transporters at other growth rates, though in rapid growth regimes, the abundance is  
 140 below our simple estimate.

141 The estimate presented in *Figure 2(A)* neglects any specifics of the regulation of carbon trans-  
 142 port system and presents a data-averaged view of how many carbohydrate transporters are present  
 143 on average. Using the diverse array of growth conditions explored in the proteomic data sets, we  
 144 can explore how individual carbon transport systems depend on the population growth rate. In  
 145 *Figure 2(B)*, we show the total number of carbohydrate transporters specific to different carbon  
 146 sources. A striking observation, shown in the top-left plot of *Figure 2(B)*, is the constancy in the  
 147 expression of the glucose-specific transport systems. Additionally, we note that the total number  
 148 of glucose-specific transporters is tightly distributed  $\approx 10^4$  per cell, the approximate number of  
 149 transporters needed to sustain rapid growth of several divisions per hour. This illustrates that *E.*  
 150 *coli* maintains a substantial number of complexes present for transporting glucose which is known  
 151 to be the preferential carbon source (*Monod, 1947; Liu et al., 2005; Aidelberg et al., 2014*).

152 It is now understood that a large number of metabolic operons are regulated with dual-input  
 153 logic gates that are only expressed when glucose concentrations are low (mediated by cyclic-AMP  
 154 receptor protein CRP) and the concentration of other carbon sources are elevated (*Gama-Castro*  
 155 *et al., 2016; Zhang et al., 2014b*). A famed example of such dual-input regulatory logic is in the regu-  
 156 lation of the *lac* operon which is only natively activated in the absence of glucose and the presence  
 157 of allolactose, an intermediate in lactose metabolism (*Jacob and Monod, 1961*), though we now  
 158 know of many other such examples (*Ireland et al., 2020; Gama-Castro et al., 2016; Belliveau et al.,*  
 159 *2018*). This illustrates that once glucose is depleted from the environment, cells have a means to  
 160 dramatically increase the abundance of the specific transporter needed to digest the next sugar  
 161 that is present. Several examples of induced expression of specific carbon-source transporters  
 162 are shown in *Figure 2(B)*. Points colored in red (labeled by red text-boxes) correspond to growth  
 163 conditions in which the specific carbon source (glycerol, xylose, or fructose) is present. These plots  
 164 show that, in the absence of the particular carbon source, expression of the transporters is main-  
 165 tained on the order of  $\sim 10^2$  per cell. However, when the transport substrate is present, expression  
 166 is induced and the transporters become highly-expressed. The grey lines in *Figure 2(B)* show the

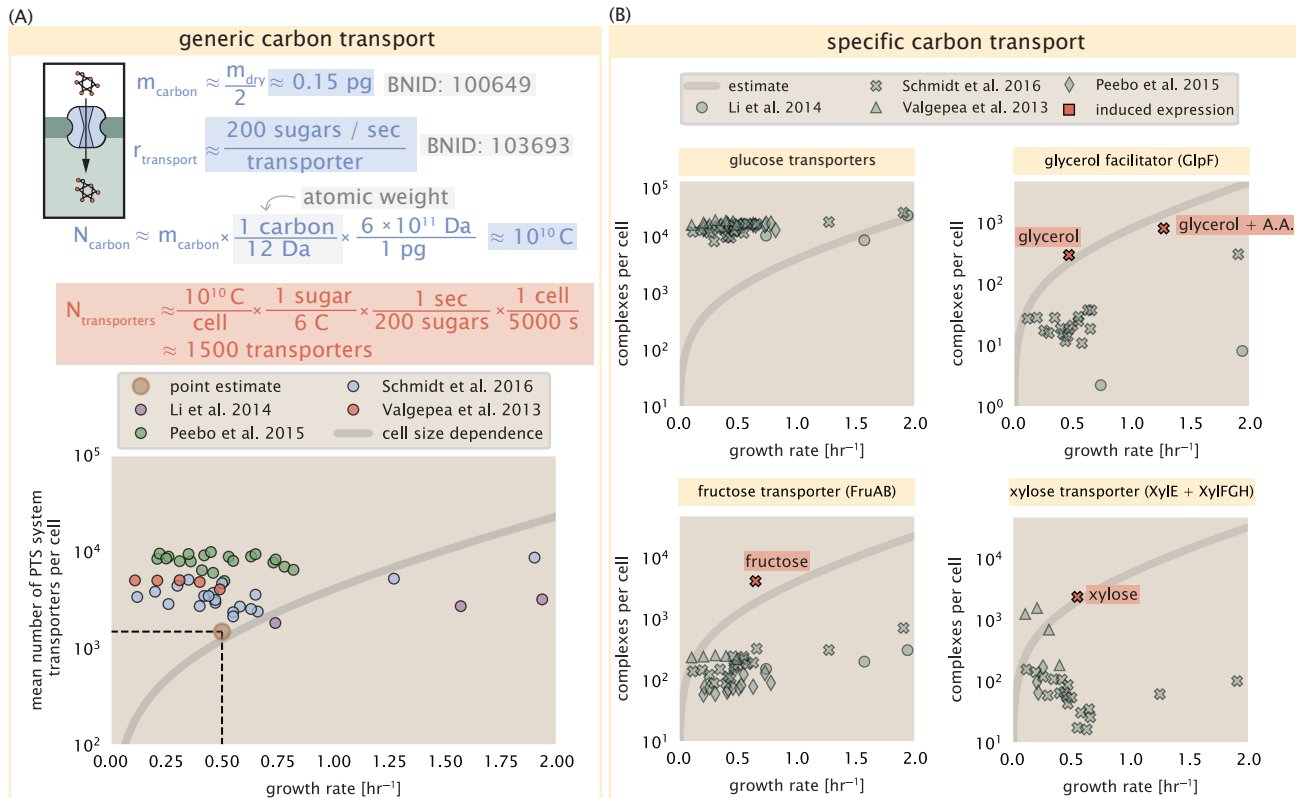


**Figure 2. The abundance of carbon transport systems across growth rates.** (A) A simple estimate for the minimum number of generic carbohydrate transport systems (top) assumes  $\approx 10^{10}$  C are needed to complete division, each transported sugar contains  $\approx 6$  C, and each transporter conducts sugar molecules at a rate of  $\approx 200$  per second. Bottom plot shows the estimated number of transporters needed at a growth rate of  $\approx 0.5$  per hr (light-brown point and dashed lines). Colored points correspond to the mean number of PTS system sugar transporters (complexes annotated with the Gene Ontology term GO:0009401) for different growth conditions across different published datasets. (B) The abundance of various specific carbon transport systems plotted as a function of the population growth rate. The rates of substrate transport to compute the continuum growth rate estimate (grey line) were 200 glucose- $s^{-1}$  (BNID: 103693, *Milo et al. (2010)*), 2000 glycerol- $s^{-1}$  (*Lu et al., 2003*), 200 fructose- $s^{-1}$  (assumed to be similar to PtsL, BNID: 103693, *Milo et al. (2010)*), and 50 xylose- $s^{-1}$  (assumed to be comparable to LacY, BNID: 103159, *Milo et al. (2010)*). Red points and highlighted text indicate conditions in which the only source of carbon in the growth medium induces expression of the transport system. Grey line in (A) and (B) represents the estimated number of transporters per cell at a continuum of growth rates.

167 estimated number of transporters needed at each growth rate to satisfy the cellular carbon re-  
 168 quirement. It is notable that in all cases, the magnitude of induced expression (shown in red) falls  
 169 close to the estimate, illustrating the ability of the cell to tune expression in response to changing  
 170 environments. Together, this generic estimation and the specific examples of induced expression  
 171 suggest that transport of carbon across the cell membrane, while critical for growth, is not the  
 172 rate-limiting step of cell division.

### 173 **Phosphorus and Sulfur Transport**

174 We now turn our attention towards other essential elements, namely phosphorus and sulfur. Phos-  
 175 phorus is critical to the cellular energy economy in the form of high-energy phosphodiester bonds  
 176 making up DNA, RNA, and the NTP energy pool as well as playing a critical role in the post-translational  
 177 modification of proteins and defining the polar-heads of lipids. In total, phosphorus makes up  
 178  $\approx 3\%$  of the cellular dry mass which in typical experimental conditions is in the form of inorganic  
 179 phosphate. The cell membrane has remarkably low permeability to this highly-charged and critical  
 180 molecule, therefore requiring the expression of active transport systems. In *E. coli*, the proton elec-  
 181 trochemical gradient across the inner membrane is leveraged to transport inorganic phosphate  
 182 into the cell (Rosenberg *et al.*, 1977). Proton-solute symporters are widespread in *E. coli* (Ramos  
 183 and Kaback, 1977; Booth *et al.*, 1979) and can have rapid transport rates of 50 to 100 molecules  
 184 per second for sugars and other solutes (BNID: 103159; 111777, Milo *et al.* (2010)). As a more  
 185 extreme example, the proton transporters in the F<sub>1</sub>-F<sub>0</sub> ATP synthase, which leverage the proton  
 186 electrochemical gradient for rotational motion, can shuttle protons across the membrane at a rate  
 187 of  $\approx 1000$  per second (BNID: 104890; 103390, (Milo *et al.*, 2010)). In *E. coli* the PitA phosphate trans-  
 188 port system has been shown to be very tightly coupled with the proton electrochemical gradient  
 189 with a 1:1 proton:phosphate stoichiometric ratio (Harris *et al.*, 2001; Feist *et al.*, 2007). Taking the  
 190 geometric mean of the aforementioned estimates gives a plausible rate of phosphate transport  
 191 on the order of 300 per second. Illustrated in *Figure 3(A)*, we can estimate that  $\approx 150$  phosphate  
 192 transporters are necessary to maintain an  $\approx 3\%$  dry mass with a 5000 s division time. This estimate  
 193 is again satisfied when we examine the observed copy numbers of PitA in proteomic data sets (plot  
 194 in *Figure 3(A)*). While our estimate is very much in line with the observed numbers, we emphasize  
 195 that this is likely a slight overestimate of the number of transporters needed as there are other  
 196 phosphorous scavenging systems, such as the ATP-dependent phosphate transporter Pst system  
 197 which we have neglected.

198 Satisfied that there are a sufficient number of phosphate transporters present in the cell, we  
 199 now turn to sulfur transport as another potentially rate limiting process. Similar to phosphate,  
 200 sulfate is highly-charged and not particularly membrane permeable, requiring active transport.  
 201 While there exists a H+/sulfate symporter in *E. coli*, it is in relatively low abundance and is not well  
 202 characterized (Zhang *et al.*, 2014a). Sulfate is predominantly acquired via the ATP-dependent ABC  
 203 transporter CysUWA system which also plays an important role in selenium transport (Sekowska  
 204 *et al.*, 2000; Sirko *et al.*, 1995). While specific kinetic details of this transport system are not readily  
 205 available, generic ATP transport systems in prokaryotes transport on the order of 1 to 10 molecules  
 206 per second (BNID: 109035, Milo *et al.* (2010)). Combining this generic transport rate, measurement  
 207 of sulfur comprising 1% of dry mass, and a 5000 second division time yields an estimate of  $\approx 1000$   
 208 CysUWA complexes per cell (*Figure 3(B)*). Once again, this estimate is in notable agreement with  
 209 proteomic data sets, suggesting that there are sufficient transporters present to acquire the nec-  
 210 essary sulfur. In a similar spirit of our estimate of phosphorus transport, we emphasize that this is  
 211 likely an overestimate of the number of necessary transporters as we have neglected other sulfur  
 212 scavenging systems that are in lower abundance.

### 213 **Limits on Transporter Expression**

214 So which, if any, of these processes may be rate limiting for growth? As suggested by *Figure 2*  
 215 (B), induced expression can lead to an order-of-magnitude (or more) increase in the amount of

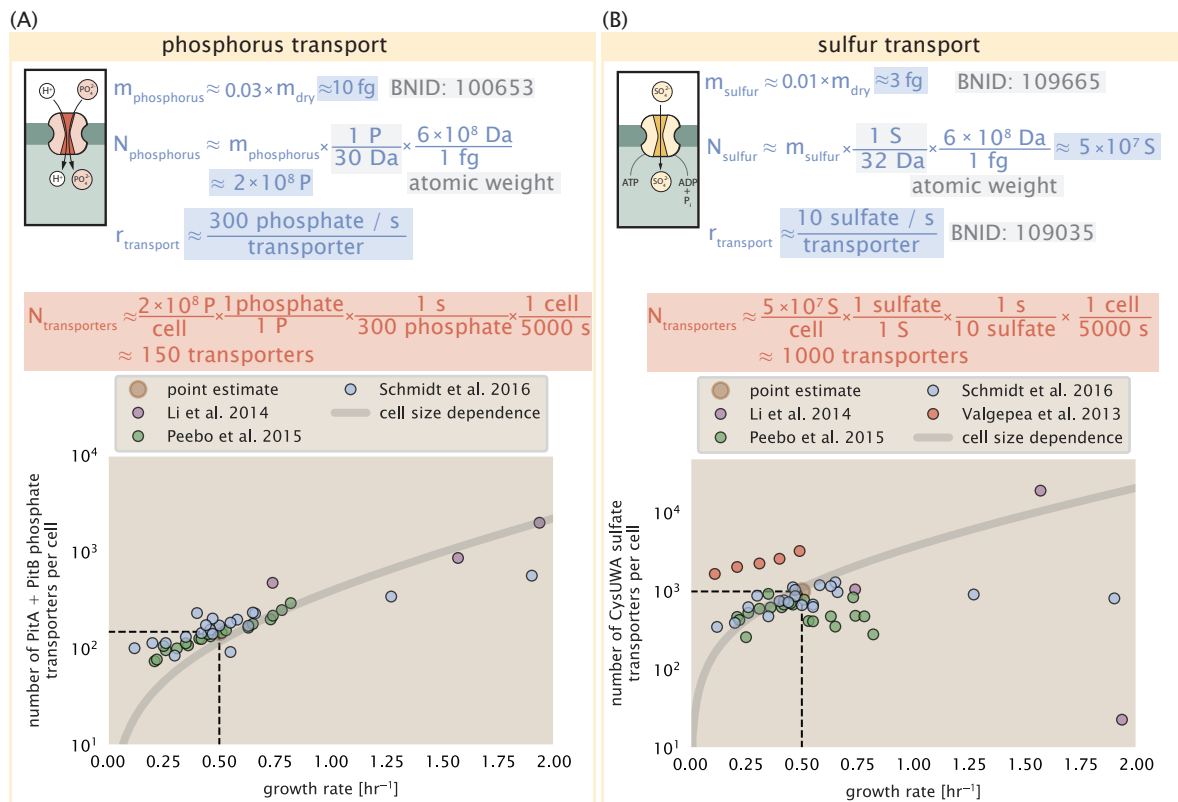


**Figure 3. Estimates and measurements of phosphate and sulfate transport systems as a function of growth rate.** (A) Estimate for the number of PitA phosphate transport systems needed to maintain a 3% phosphorus *E. coli* dry mass. Points in plot correspond to the total number of PitA transporters per cell. (B) Estimate of the number of CysUWA complexes necessary to maintain a 1% sulfur *E. coli* dry mass. Points in plot correspond to average number of CysUWA transporter complexes that can be formed given the transporter stoichiometry [CysA]<sub>2</sub>[CysU][CysW][Sbp/CysP]. Grey line in (A) and (B) represents the estimated number of transporters per cell at a continuum of growth rates.

216 transporters needed to facilitate transport. Thus, if acquisition of nutrients was the limiting state  
 217 in cell division, could expression simply be increased to accommodate faster growth? A way to  
 218 approach this question is to compute the amount of space in the bacterial membrane that could  
 219 be occupied by nutrient transporters. Considering a rule-of-thumb for the surface area of *E. coli* of  
 220 about  $6 \mu\text{m}^2$  (BNID: 101792, *Milo et al. (2010)*), we expect an areal density for 1000 transporters to  
 221 be approximately 200 transporters/ $\mu\text{m}^2$ . For a typical transporter occupying about  $50 \text{ nm}^2/\text{dimer}$ ,  
 222 this amounts to about only 1 percent of the total inner membrane (*Szenk et al., 2017*). In addition,  
 223 bacterial cell membranes typically have densities of  $10^5$  proteins/ $\mu\text{m}^2$  (*Phillips, 2018*), implying that  
 224 the cell could accommodate more transporters of a variety of species if it were rate limiting. As we  
 225 will see in the next section, however, occupancy of the membrane can impose other limits on the  
 226 rate of energy production.

## 227 Energy Production

228 While the transport of nutrients is required to build new cell mass, the metabolic pathways both  
 229 consume and generate energy in the form of NTPs. The high-energy phosphodiester bonds of  
 230 (primarily) ATP power a variety of cellular processes that drive biological systems away from ther-  
 231 modynamic equilibrium. The next set of processes we hypothesize might control the rate of cell  
 232 division considers the energy budget of a dividing cell in terms of the synthesis of ATP from ADP  
 233 and inorganic phosphate as well as maintenance of the electrochemical proton gradient which  
 234 powers it.

## 235 ATP Synthesis

236 Hydrolysis of the terminal phosphodiester bond of ATP forming ADP and an inorganic phosphate is  
 237 a kinetic driving force in a wide array of biochemical reactions. One such reaction is the formation  
 238 of peptide bonds during translation which requires  $\approx 2$  ATPs for the charging of an amino acid  
 239 to the tRNA and  $\approx 2$  ATP equivalents for the formation of the peptide bond between amino acids.  
 240 Considering the ATP costs associated with error correction and post-translational modifications  
 241 of proteins, we can make the approximation that each peptide bond has a net cost of  $\approx 5$  ATP  
 242 (BNID: 107782, *Milo et al. (2010)*). In total, the energetic costs of peptide bond formation consume  
 243  $\approx 80\%$  of the cells ATP budget (BNID: 107782; 106158; 101637; 111918, *Milo et al. (2010); Lynch*  
*and Marinov (2015); Stouthamer (1973)*). The pool of ATP is produced by the F<sub>1</sub>-F<sub>0</sub> ATP synthase  
 245 – a membrane-bound rotary motor which under ideal conditions can yield  $\approx 300$  ATP per second  
 246 (BNID: 114701; *Milo et al. (2010); Weber and Senior (2003)*).

247 To estimate the total number of ATP equivalents consumed during a cell cycle, we will make  
 248 the approximation that there are  $\approx 3 \times 10^6$  proteins per cell with an average protein length of  $\approx 300$   
 249 peptide bonds (BNID: 115702; 108986; 104877, *Milo et al. (2010)*). Taking these values together,  
 250 we estimate that the typical *E. coli* cell consumes  $\approx 5 \times 10^9$  ATP per cell cycle on protein synthesis  
 251 alone and  $\approx 6 \times 10^9$  ATP in total. Assuming that the ATP synthases are operating at their fastest  
 252 possible rate,  $\approx 3000$  ATP synthases are needed to keep up with the energy demands of the cell.  
 253 This estimate and a comparison with the data are shown in *Figure 4* (A). Despite our assumption  
 254 of maximal ATP production rate per synthase and approximation of all NTP consuming reactions  
 255 being the same as ATP, we find that an estimate of a few thousand complete synthases per cell  
 256 to agree well with the experimental data. Much as we did for the estimates of transporter copy  
 257 number in the previous section, we can generalize this estimation to consider a continuum of  
 258 growth rates rather than a point estimate of 5000 s, indicated by the gray lines in *Figure 4*, and find  
 259 that this approach adequately describes the observed growth rate dependence.

260 If the direct production of ATP was a rate limiting step for growth, could the cell simply express  
 261 more ATP synthase complexes? This requires us to consider several features of cellular physiology,  
 262 namely the physical space on the inner membrane as well as the ability to maintain the proton  
 263 chemical gradient leveraged by the synthase to drive ATP production out of equilibrium.

**264 Generating the Proton Electrochemical Gradient**

265 In order to produce ATP, the F<sub>1</sub>-F<sub>0</sub> ATP synthase itself must consume energy. Rather than burning  
 266 through its own product, this intricate macromolecular machine has evolved to exploit the elec-  
 267 trochemical potential established across the inner membrane through cellular respiration. This  
 268 electrochemical gradient is manifest by the pumping of protons into the intermembrane space via  
 269 the electron transport chains as they reduce NADH. In *E. coli*, this potential difference is  $\approx -200$  mV  
 270 (BNID: 102120, *Milo et al. (2010)*). A simple estimate of the inner membrane as a capacitor with a  
 271 working voltage of -200 mV (as performed in the Supplemental Information) reveals that  $\approx 2 \times 10^4$   
 272 protons must be present in the intermembrane space.

273 However, the constant rotation of the ATP synthases would rapidly abolish this potential dif-  
 274 ference if it were not being actively maintained. To undergo a complete rotation (and produce a  
 275 single ATP), the F<sub>1</sub>-F<sub>0</sub> ATP synthase must shuttle  $\approx 4$  protons across the membrane into the cytosol  
 276 (BNID: 103390, *Milo et al. (2010)*). With  $\approx 3000$  ATP synthases each generating 300 ATP per second,  
 277 the  $2 \times 10^4$  protons establishing the 200 mV potential would be consumed in only a few millisec-  
 278 onds. This brings us to our next estimate: how many electron transport complexes are needed to  
 279 support the consumption rate of the ATP synthases?

280 The electrochemistry of the electron transport complexes of *E. coli* have been the subject of  
 281 intense biochemical and biophysical study over the past half century (*Ingledew and Poole, 1984;*  
*282 Khademian and Imlay, 2017; Cox et al., 1970; Henkel et al., 2014*). A recent work (*Szenk et al.,*  
*283 2017*) examined the respiratory capacity of the *E. coli* electron transport complexes using struc-  
 284 tural and biochemical data, revealing that each electron transport chain rapidly pumps protons  
 285 into the intermembrane space at a clip of  $\approx 1500$  protons per second (BIND: 114704; 114687, *Milo*  
*286 et al. (2010)*). Using our estimate of the number of ATP synthases required per cell (*Figure 4(A)*),  
 287 coupled with these recent measurements, we estimate that  $\approx 1000$  electron transport complexes  
 288 would be necessary to facilitate the  $\approx 4 \times 10^6$  protons per second diet of the cellular ATP synthases.  
 289 This estimate (along with a generalization to the entire range of observed growth rates) is in agree-  
 290 ment with the number of complexes identified in the proteomic datasets (plot in *Figure 4(B)*). This  
 291 suggests that every ATP synthase must be accompanied by  $\approx 1$  functional electron transport chain.  
 292 Again, if this were a rate limiting process for bacterial growth, one must conclude that it is not  
 293 possible for the cell to simply increase the production of both the number of electron transport  
 294 chain complexes as well as ATP synthases. As both of these components only function bound to  
 295 the inner membrane, we now turn our attention towards the available space in the membrane as  
 296 well as surface-area-to-volume constraints.

**297 Energy Production in a Crowded Membrane.**

298 For each protein considered so far, the data shows that in general their numbers increase with  
 299 growth rate. This is in part a consequence of the increase in cell length and width at that is common  
 300 to many rod-shaped bacteria at faster growth rates (*Ojikic et al., 2019; Harris and Theriot, 2018*).  
 301 For the particular case of *E. coli*, the total cellular protein and cell size increase logarithmically  
 302 with growth rate (*Schaechter et al., 1958; Si et al., 2017*). Indeed, this is one reason why we have  
 303 considered only a single, common growth condition across all our estimates so far. Such a scaling  
 304 will require that the total number of proteins and net demand on resources also grow in proportion  
 305 to the increase in cell size divided by the cell's doubling time. Recall however that each transport  
 306 process, as well as the ATP production via respiration, is performed at the bacterial membrane.  
 307 This means that their maximum productivity can only increase in proportion to the cell's surface  
 308 area divided by the cell doubling time. This difference in scaling would vary in proportion to the  
 309 surface area-to-volume (S/V) ratio.

310 While we found that there was more than sufficient membrane real estate for carbon intake in  
 311 our earlier estimate, the total number of ATP synthases and electron chain transport complexes  
 312 both exhibit a clear increase in copy number with growth rate, reaching in excess of  $10^4$  copies per  
 313 cell (*Figure 4*). Here we consider the consequences of this S/V ratio scaling in more detail.

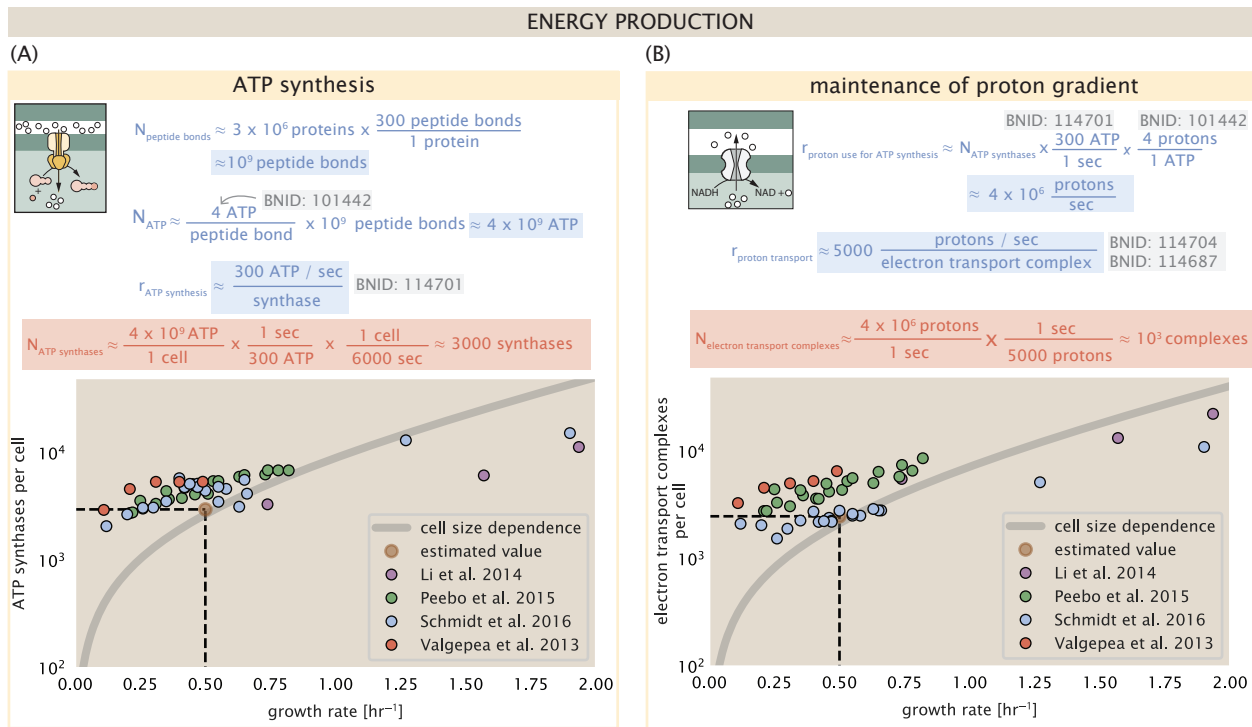


**Figure 4. The abundance of F<sub>1</sub>-F<sub>0</sub> ATP synthases and electron transport chain complexes as a function of growth rate.** (A) Estimate of the number of F<sub>1</sub>-F<sub>0</sub> ATP synthase complexes needed to accommodate peptide bond formation and other NTP dependent processes. Points in plot correspond to the mean number of complete F<sub>1</sub>-F<sub>0</sub> ATP synthase complexes that can be formed given proteomic measurements and the subunit stoichiometry [AtpE]<sub>10</sub>[AtpF]<sub>2</sub>[AtpB][AtpC][AtpH][AtpA]<sub>3</sub>[AtpG][AtpD]<sub>3</sub>. (B) Estimate of the number of electron transport chain complexes needed to maintain a membrane potential of -200 mV given estimate of number of F<sub>1</sub>-F<sub>0</sub> ATP synthases from (A). Points in plot correspond to the average number of complexes identified as being involved in aerobic respiration by the Gene Ontology identifier GO:0019646 that could be formed given proteomic observations. These complexes include cytochromes *bd1* ([CydA][CydB][CydX][CydH]), *bdII* ([AppC][AppB]), *bo3*, ([CyoD][CyoA][CyoB][CyoC]) and NADH:quinone oxioreductase I ([NuoA][NuoH][NuoJ][NuoK][NuoL][NuoM][NuoN][NuoB][NuoC][NuoE][NuoF][NuoG][NuoI]) and II ([Ndh]). Grey lines in both (A) and (B) correspond to the estimate procedure described, but applied to a continuum of growth rates. We direct the reader to the Supporting Information for a more thorough description of this approach.

314 In our estimate of ATP production above we found that a cell demands about  $6 \times 10^9$  ATP or  $10^6$   
 315 ATP/s. With a cell volume of roughly 1 fL, this corresponds to about  $2 \times 10^{10}$  ATP per fL of cell volume,  
 316 in line with previous estimates (*Stouthamer and Bettenhausen, 1977; Szenk et al., 2017*). In **Figure 5**(A) we plot this ATP demand as a function of the S/V ratio in green, where we have considered  
 317 a range of cell shapes from spherical to rod-shaped with an aspect ratio (length/width) equal to 4  
 318 (See appendix for calculations of cell volume and surface area). In order to consider the maximum  
 319 power that could be produced, we consider the amount of ATP that can be generated by a membrane  
 320 filled with ATP synthase and electron transport complexes, which provides a maximal production  
 321 of about 3 ATP / (nm<sup>2</sup>·s) (*Szenk et al., 2017*). This is shown in blue in **Figure 5**(A), which shows that  
 322 at least for the growth rates observed, the energy demand is roughly an order of magnitude less.  
 323

324 Interestingly, *Szenk et al. (2017)* also found that ATP production by respiration is less efficient  
 325 than by fermentation per membrane area occupied due to the additional proteins of the electron  
 326 transport chain. This suggests that even under anaerobic growth, there will be sufficient mem-  
 327 brane space for ATP production in general.

328 While this serves to highlight the diminishing capacity to provide resources to grow if the cell  
 329 increases in size (and its S/V decreases), the blue region in **Figure 5**(A) represents a somewhat  
 330 unachievable limit since the inner membrane must also include other proteins such as those re-  
 331 quired for lipid and membrane synthesis. To gain insight, we used the proteomic data to look at  
 332 the distribution of proteins on the inner membrane. Here we use Gene Ontology (GO) annotations  
 333 (*Ashburner et al., 2000; The Gene Ontology Consortium, 2018*) to identify all proteins embedded  
 334 or peripheral to the inner membrane (GO term: 0005886). Those associated but not membrane-  
 335 bound include proteins like MreB and FtsZ, that traverse the inner membrane by treadmilling and  
 336 must nonetheless be considered as a vital component occupying space on the membrane. In **Fig-**  
 337 **ure 5**(B), we find that the total protein mass per  $\mu\text{m}^2$  is relatively constant with growth rate. Inter-  
 338 estingly, when we consider the distribution of proteins grouped by their Clusters of Orthologous  
 339 Groups (COG) (*Tatusov et al., 2000*), the relative abundance for those in metabolism (including ATP  
 340 synthesis via respiration) is also relatively constant.

### 341 Function of the Central Dogma

342 Up to this point, we have considered a variety of transport and biosynthetic processes that are  
 343 critical to acquiring and generating new cell mass. While there are of course many other metabolic  
 344 processes we could consider and perform estimates of (such as the components of fermentative  
 345 versus aerobic respiration), we now turn our focus to some of the most central processes which  
 346 *must* be undertaken irrespective of the growth conditions – the processes of the central dogma.

### 347 DNA

348 Most bacteria (including *E. coli*) harbor a single, circular chromosome and can have extra-chromosomal  
 349 plasmids up to  $\sim 100$  kbp in length. We will focus our quantitative thinking solely on the chromo-  
 350 some of *E. coli* which harbors  $\approx 5000$  genes and  $\approx 5 \times 10^6$  base pairs. To successfully divide and  
 351 produce viable progeny, this chromosome must be faithfully replicated and segregated into each  
 352 nascent cell. We again rely on the near century of literature in molecular biology to provide some  
 353 insight on the rates and mechanics of the replicative feat as well as the production of the required  
 354 starting materials, dNTPs.

### 355 dNTP synthesis

356 We begin our exploration of DNA replication by examining the production of the deoxyribonucleotide  
 357 triphosphates (dNTPs). The four major dNTPs (dATP, dTTP, dCTP, and dGTP) are synthesized *de*  
 358 *novo* in separate pathways, requiring different building blocks. However, a critical step present in  
 359 all dNTP synthesis pathways is the conversion from ribonucleotide to deoxyribonucleotide via the  
 360 removal of the 3' hydroxyl group of the ribose ring (*Rudd et al., 2016*). This reaction is mediated  
 361 by a class of enzymes termed ribonucleotide reductases, of which *E. coli* possesses two aerobically

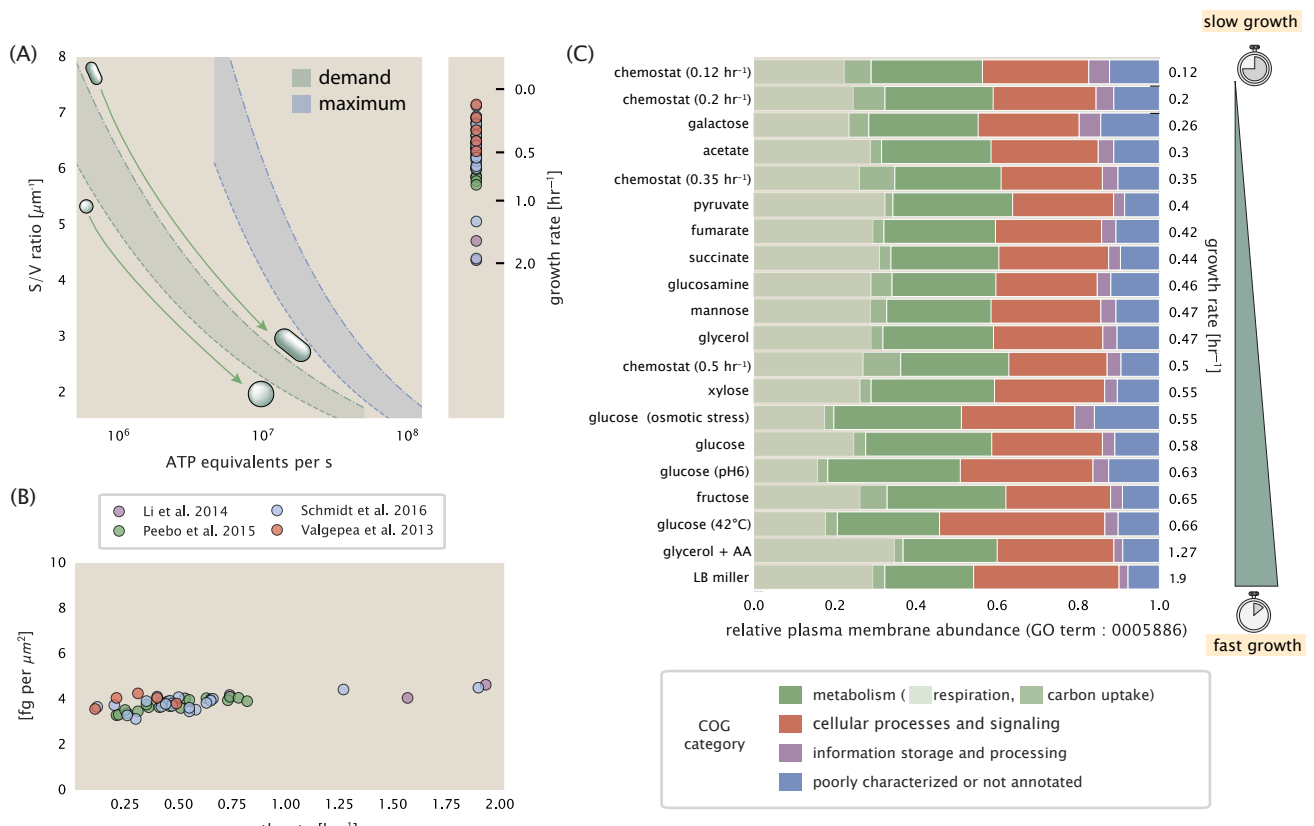


**Figure 5. Influence of cell size and S/V ratio on ATP production and inner membrane composition.** (A) Scaling of ATP demand and maximum ATP production as a function of S/V ratio. Cell volumes of 0.5 fL to 50 fL were considered, with the dashed (—) line corresponding to a sphere and the dash-dot line (---) reflecting a rod-shaped bacterium like *E. coli* with a typical aspect ratio (length / width) of 0.4 (Shi et al., 2018). Approximately 50% of the bacterial inner membrane is assumed to be protein, with the remainder lipid. (B) Total protein mass calculated for proteins with inner membrane annotation (GO term: 0005886). (C) Relative protein abundances by mass based on COG annotation. Metabolic proteins are further separated into respiration ( $F_1$ - $F_0$  ATP synthase, NADH dehydrogenase I, succinate:quinone oxidoreductase, cytochrome bo<sub>3</sub> ubiquinol oxidase, cytochrome bd-I ubiquinol oxidase) and carbohydrate transport (GO term: GO:0008643). Note that the elongation factor EF-Tu can also associate with the inner membrane, but was excluded in this analysis due to its high relative abundance (roughly identical to the total mass shown in part (B)).

362 active complexes (termed I and II) and a single anaerobically active enzyme. Due to their peculiar  
 363 formation of a radical intermediate, these enzymes have received much biochemical, kinetic, and  
 364 structural characterization. One such work (**Ge et al., 2003**) performed a detailed *in vitro* measure-  
 365 ment of the steady-state kinetic rates of these complexes, revealing a turnover rate of  $\approx 10$  dNTP  
 366 per second.

367 Since this reaction is central to the synthesis of all dNTPs, it is reasonable to consider the abun-  
 368 dence of these complexes is a measure of the total dNTP production in *E. coli*. Illustrated schemati-  
 369 cally in **Figure 6** (A), we consider the fact that to replicate the cell's genome, on the order of  $\approx 10^7$   
 370 dNTPs must be synthesized. Assuming a production rate of 10 per second per ribonucleotide  
 371 reductase complex and a cell division time of 5000 seconds, we arrive at an estimate of  $\approx 200$   
 372 complexes needed per cell. As shown in the bottom panel of **Figure 6** (A), this estimate agrees  
 373 with the experimental measurements of these complexes abundances within  $\approx 1/2$  an order of  
 374 magnitude. Extension of this estimate across a continuum of growth rate, including the fact that  
 375 multiple chromosomes can be replicated at a given time, is shown as a grey transparent line in  
 376 **Figure 6** (A). Similarly to our point estimate, this refinement agrees well with the data, accurately  
 377 describing both the magnitude of the complex abundance and the dependence on growth rate.

378 Recent work has revealed that during replication, the ribonucleotide reductase complexes co-  
 379 alesce to form discrete foci colocalized with the DNA replisome complex (**Sánchez-Romero et al.,**  
 380 **2011**). This is particularly pronounced in conditions where growth is slow, indicating that spatial  
 381 organization and regulation of the activity of the complexes plays an important role.

### 382 DNA Replication

383 We now turn our focus to the integration of these dNTP building blocks into the replicated chromo-  
 384 some strand via the DNA polymerase. Replication is initiated at a single region of the chromosome  
 385 termed the *oriC* locus at which a pair of DNA polymerases bind and begin their high-fidelity repli-  
 386 cation of the genome in opposite directions. Assuming equivalence between the two replication  
 387 forks, this means that the two DNA polymerase complexes (termed replisomes) meet at the mid-  
 388 way point of the circular chromosome termed the *ter* locus. The kinetics of the five types of DNA  
 389 polymerases (I – V) have been intensely studied, revealing that DNA polymerase III performs the  
 390 high fidelity processive replication of the genome with the other "accessory" polymerases playing  
 391 auxiliary roles (**Fijalkowska et al., 2012**). *In vitro* measurements have shown that DNA Polymerase  
 392 III copies DNA at a rate of  $\approx 600$  nucleotides per second (BNID: 104120, **Milo et al. (2010)**). There-  
 393 fore, to replicate a single chromosome, two replisomes (containing two DNA polymerase III each)  
 394 moving at their maximal rate would copy the entire genome in  $\approx 4000$  s. Thus, with a division time  
 395 of 5000 s (our "typical" growth rate for the purposes of this work), there is sufficient time for a pair  
 396 of replisomes complexes to replicate the entire genome. However, this estimate implies that 4000  
 397 s would be the upper-limit time scale for bacterial division which is at odds with the familiar 20  
 398 minute (1200 s) doubling time of *E. coli* in rich medium.

399 It is well known that *E. coli* can parallelize its DNA replication such that multiple chromosomes  
 400 are being replicated at once, with as many as 10 - 12 replication forks at a given time (**Bremer**  
 401 **and Dennis, 2008; Si et al., 2017**). Thus, even in rapidly growing cultures, we expect only a few  
 402 polymerases ( $\approx 10$ ) are needed to replicate the chromosome per cell doubling. However, as shown  
 403 in **Figure 6** (B), DNA polymerase III is nearly an order of magnitude more abundant. This  
 404 discrepancy can be understood by considering its binding constant to DNA. DNA polymerase III is  
 405 highly processive, facilitated by a strong affinity of the complex to the DNA. *In vitro* biochemical  
 406 characterization has quantified the  $K_D$  of DNA polymerase III holoenzyme to single-stranded and  
 407 double-stranded DNA to be 50 and 200 nM, respectively (**Ason et al., 2000**). The bottom plot in  
 408 **Figure 6** (B) shows that the concentration of the DNA polymerase III across all data sets and growth  
 409 conditions is within this range. Thus, while the copy number of the DNA polymerase III is in excess  
 410 of the strict number required to replicate the genome, its copy number appears to vary such that its  
 411 concentration is approximately equal to the dissociation constant to the DNA. While the processes

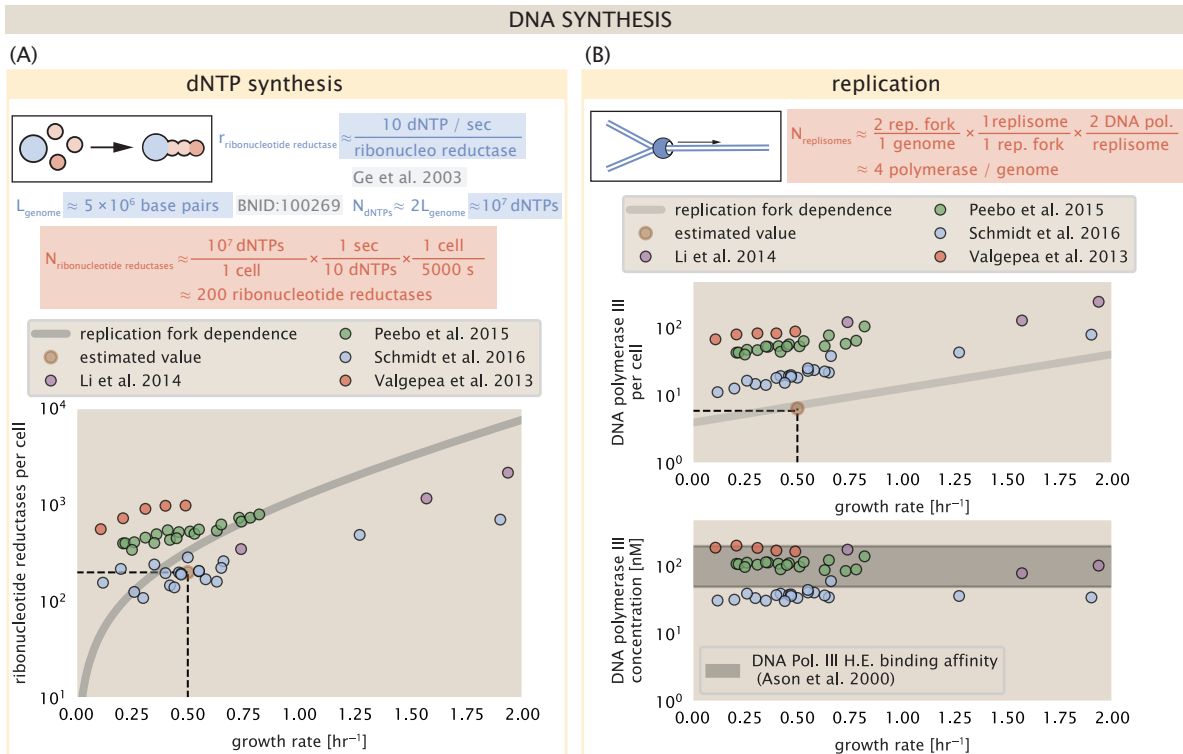


**Figure 6. Complex abundance estimates for dNTP synthesis and DNA replication.** (A) Estimate of the number of ribonucleotide reductase enzymes needed to facilitate the synthesis of  $\approx 10^7$  dNTPs over the course of a 5000 second generation time. Points in the plot correspond to the total number of ribonucleotide reductase I ( $[\text{NrdA}]_2[\text{NrdB}]_2$ ) and ribonucleotide reductase II ( $[\text{NrdE}]_2[\text{NrdF}]_2$ ) complexes. (B) An estimate for the minimum number of DNA polymerase holoenzyme complexes needed to facilitate replication of a single genome. Points in the top plot correspond to the total number of DNA polymerase III holoenzyme complexes ( $[\text{DnaE}]_3[\text{DnaQ}]_3[\text{HolE}]_3[\text{DnaX}]_5[\text{HolB}][\text{HolA}][\text{DnaN}]_4[\text{HolC}]_4[\text{HolD}]_4$ ) per cell. Bottom plot shows the effective concentration of DNA polymerase III holoenzyme given cell volumes calculated from the growth rate as in *Si et al. (2019)* (See Supplemental Information Section 4). Grey lines in (A) and top panel of (B) show the estimated number of complexes needed as a function of growth, the details of which are described in the Supplemental Information.

regulating the initiation of DNA replication are complex and involve more than just the holoenzyme, these data indicate that the kinetics of replication rather than the explicit copy number of the DNA polymerase III holoenzyme is the more relevant feature of DNA replication to consider. In light of this, the data in **Figure 6(B)** suggests that for bacteria like *E. coli*, DNA replication does not represent a rate-limiting step in cell division. However, it is worth noting that for bacterium like *C. crescentus* whose chromosomal replication is initiated only once per cell cycle (*Jensen et al., 2001*), the time to double their chromosome likely represents an upper limit to their growth rate.

#### RNA Synthesis

With the machinery governing the replication of the genome accounted for, we now turn our attention to the next stage of the central dogma – the transcription of DNA to form RNA. We primarily consider three major groupings of RNA, namely the RNA associated with ribosomes (rRNA), the RNA encoding the amino-acid sequence of proteins (mRNA), and the RNA which links codon sequence to amino-acid identity during translation (tRNA). Despite the varied function of these RNA species, they share a commonality in that they are transcribed from DNA via the action of RNA polymerase. In the coming paragraphs, we will consider the synthesis of RNA as a rate limiting step in bacterial division by estimating how many RNA polymerases must be present to synthesize all necessary rRNA, mRNA, and tRNA.

#### rRNA

We begin with an estimation of the number of RNA polymerases needed to synthesize the rRNA that serve as catalytic and structural elements of the ribosome. Each ribosome contains three rRNA molecules of lengths 120, 1542, and 2904 nucleotides (BNID: 108093, *Milo et al. (2010)*), meaning each ribosome contains  $\approx 4500$  nucleotides. As the *E. coli* RNA polymerase transcribes DNA to RNA at a rate of  $\approx 40$  nucleotides per second (BNID: 101904, *Milo et al. (2010)*), it takes a single RNA polymerase  $\approx 100$  s to synthesize the RNA needed to form a single functional ribosome. Therefore, in a 5000 s division time, a single RNA polymerase transcribing rRNA at a time would result in only  $\approx 50$  functional ribosomal rRNA units – far below the observed number of  $\approx 10^4$  ribosomes per cell.

Of course, there can be more than one RNA polymerase transcribing the rRNA genes at any given time. To elucidate the *maximum* number of rRNA units that can be synthesized given a single copy of each rRNA gene, we will consider a hypothesis in which the rRNA operon is completely tiled with RNA polymerase. *In vivo* measurements of the kinetics of rRNA transcription have revealed that RNA polymerases are loaded onto the promoter of an rRNA gene at a rate of  $\approx 1$  per second (BNID: 111997; 102362, *Milo et al. (2010)*). If RNA polymerases are being constantly loaded on to the rRNA genes at this rate, then we can assume that  $\approx 1$  functional rRNA unit is synthesized per second. With a 5000 second division time, this hypothesis leads to a maximal value of 5000 functional rRNA units, still undershooting the observed number of  $10^4$  ribosomes per cell.

*E. coli* has evolved a clever mechanism to surpass this kinetic limit for the rate of rRNA production. Rather than having only one copy of each rRNA gene, *E. coli* has seven copies of the operon (BIND: 100352, *Milo et al. (2010)*) four of which are localized directly adjacent to the origin of replication (*Birnbaum and Kaplan, 1971*). As fast growth also implies an increased gene dosage due to parallelized chromosomal replication, the total number of rRNA genes can be on the order of  $\approx 10 - 70$  copies at moderate to fast growth rates (*Stevenson and Schmidt, 2004*). Using our standard time scale of a 5000 second division time, we can make the lower-bound estimate that the typical cell will have 7 copies of the rRNA operon. Synthesizing one functional rRNA unit per second per rRNA operon, a total of  $4 \times 10^4$  rRNA units can be synthesized, comfortably above the observed number of ribosomes per cell.

How many RNA polymerases are then needed to constantly transcribe 7 copies of the rRNA genes? We approach this estimate by considering the maximum number of RNA polymerases tiled along the rRNA genes with a loading rate of 1 per second and a transcription rate of 40 nucleotides per second. Considering that a RNA polymerase has a physical footprint of approximately 40 nu-

**461** cleotides (BNID: 107873, *Milo et al. (2010)*), we can expect  $\approx 1$  RNA polymerase per 80 nucleotides.  
**462** With a total length of  $\approx 4500$  nucleotides per operon and 7 operons per cell, the maximum number  
**463** of RNA polymerases that can be transcribing rRNA at any given time is  $\approx 400$ . As we will see in the  
**464** coming sections, the synthesis of rRNA is the dominant requirement of the RNA polymerase pool.

**465** mRNA

**466** To form a functional protein, all protein coding genes must first be transcribed from DNA to form  
**467** an mRNA molecule. While each protein requires an mRNA blueprint, many copies of the protein  
**468** can be synthesized from a single mRNA. Factors such as strength of the ribosomal binding site,  
**469** mRNA stability, and rare codon usage frequency dictate the number of proteins that can be made  
**470** from a single mRNA, with yields ranging from  $10^1$  to  $10^4$  (BNID: 104186; 100196; 106254, *Milo et al.*  
**471** (2010)). Computing the geometric mean of this range yields  $\approx 1000$  proteins synthesized per mRNA,  
**472** a value that agrees with experimental measurements of the number of proteins per cell ( $\approx 3 \times 10^6$ ,  
**473** BNID: 100088, *Milo et al. (2010)*) and total number of mRNA per cell ( $\approx 3 \times 10^3$ , BNID:100064, *Milo*  
**474** *et al. (2010)*).

**475** This estimation captures the *steady-state* mRNA copy number, meaning that at any given time,  
**476** there will exist approximately 3000 unique mRNA molecules. To determine the *total* number of  
**477** mRNA that need to be synthesized over the cell's lifetime, we must consider degradation of the  
**478** mRNA. In most bacteria, mRNAs are rather unstable with life times on the order of several minutes  
**479** (BNID: 104324; 106253; 111927; 111998, *Milo et al. (2010)*). For convenience, we assume that the  
**480** typical mRNA in our cell of interest has a typical lifetime of  $\approx 300$  seconds. Using this value, we  
**481** can determine the total mRNA production rate to maintain a steady-state copy number of 3000  
**482** mRNA per cell. While we direct the reader to the appendix for a more detailed discussion of mRNA  
**483** transcriptional dynamics, we state here that the total mRNA production rate must be on the order  
**484** of  $\approx 15$  mRNA per second. In *E. coli*, the average protein is  $\approx 300$  amino acids in length (BNID:  
**485** 108986; *Milo et al. (2010)*), meaning that the corresponding mRNA is  $\approx 900$  nucleotides which we  
**486** will further approximate as  $\approx 1000$  nucleotides to account for the non-protein coding regions on  
**487** the 5' and 3' ends. This means that the cell must have enough RNA polymerase molecules about  
**488** to sustain a transcription rate of  $\approx 1.5 \times 10^4$  nucleotides per second. Knowing that a single RNA  
**489** polymerase polymerizes RNA at a clip of 40 nucleotides per second, we arrive at a comfortable  
**490** estimate of  $\approx 250$  RNA polymerase complexes needed to satisfy the mRNA demands of the cell. It  
**491** is worth noting that this number is approximately half of that required to synthesize enough rRNA,  
**492** as we saw in the previous section. We find this to be a striking result as these 250 RNA polymerase  
**493** molecules are responsible for the transcription of the  $\approx 4000$  protein coding genes that are not  
**494** ribosome associated.

**495** tRNA

**496** The final class of RNA molecules worthy of quantitative consideration is the the pool of tRNAs  
**497** used during translation to map codon sequence to amino acid identity. Unlike mRNA or rRNA,  
**498** each individual tRNA is remarkably short, ranging from 70 to 95 nucleotides each (BNID: 109645;  
**499** 102340, *Milo et al. (2010)*). What they lack in length, they make up for in abundance. There are  
**500** many measurements of the size of the *E. coli* tRNA pool, ranging from  $\approx 6 \times 10^4$  (BNID:105280, *Milo*  
**501** *et al. (2010)*) to  $\approx 4 \times 10^5$  (BNID: 108611). To test tRNA synthesis as a possible growth-rate limiting  
**502** stage, we will err towards a higher abundance of  $\approx 4 \times 10^5$  per cell. Combining the abundance and  
**503** tRNA length measurements, we make the estimate that  $\approx 5 \times 10^7$  nucleotides are sequestered in  
**504** tRNA per cell. Unlike mRNA, tRNA is remarkably stable with typical lifetimes *in vivo* on the order of  
**505**  $\approx 48$  hours (*Abelson et al., 1974; Svenningsen et al., 2017*) – well beyond the timescale of division.  
**506** Once again using our rule-of-thumb for the rate of transcription to be 40 nucleotides per second  
**507** and assuming a division time of  $\approx 5000$  seconds, we arrive at an estimate of  $\approx 150$  RNA polymerases  
**508** to synthesize enough tRNA. This requirement pales in comparison to the number of polymerases  
**509** needed to generate the rRNA and mRNA pools and can be neglected as a significant transcriptional

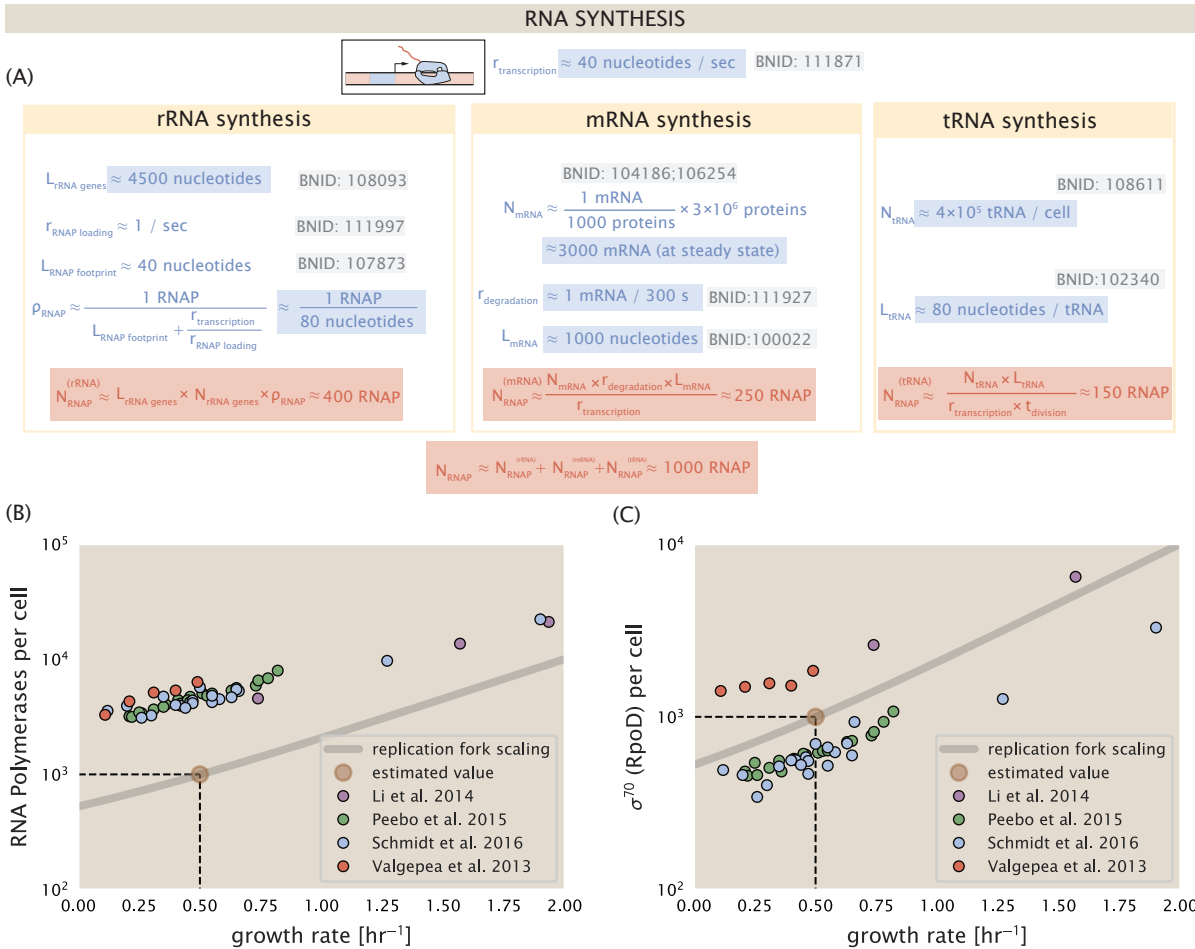


**Figure 7. Estimation of the RNA polymerase demand and comparison with experimental data.** (A)

Estimations for the number of RNA polymerase needed to synthesize sufficient quantities of rRNA, mRNA, and tRNA from left to right, respectively. Bionumber Identifiers (BNIDs) are provided for key quantities used in the estimates. (B) The RNA polymerase core enzyme copy number as a function of growth rate. Colored points correspond to the average number RNA polymerase core enzymes that could be formed given a subunit stoichiometry of  $[RpoA]_2[RpoC][RpoB]$ . (C) The abundance of  $\sigma^{70}$  as a function of growth rate. Estimated value for the number of RNAP is shown in (B) and (C) as a translucent brown point at a growth rate of  $0.5 \text{ hr}^{-1}$ .

510 burden.

#### 511 RNA Polymerase and $\sigma$ -factor Abundance

512 These estimates, summarized in **Figure 7 (A)**, reveal that synthesis of rRNA and mRNA are the domi-  
513 nant RNA species synthesized by RNA polymerase, suggesting the need for  $\approx 700$  RNA polymerases  
514 per cell. As is revealed in **Figure 7 (B)**, this estimate is about an order of magnitude below the ob-  
515 served number of RNA polymerase complexes per cell ( $\approx 5000 - 7000$ ). The disagreement between  
516 the estimated number of RNA polymerases and these observations are at least consistent with  
517 recent literature revealing that  $\approx 80\%$  of RNA polymerases in *E. coli* are not transcriptionally active  
518 (*Patrick et al., 2015*). Our estimate ignores the possibility that some fraction is only nonspecifically  
519 bound to DNA, as well as the obstacles that RNA polymerase and DNA polymerase present for each  
520 other as they move along the DNA (*Finkelstein and Greene, 2013*).

521 In addition, it is also vital to consider the role of  $\sigma$ -factors which help RNA polymerase identify  
522 and bind to transcriptional start sites (*Browning and Busby, 2016*). Here we consider  $\sigma^{70}$  (RpoD)  
523 which is the dominant "general-purpose"  $\sigma$ -factor in *E. coli*. While initially thought of as being solely

involved in transcriptional initiation, the past two decades of single-molecule work has revealed a more multipurpose role for  $\sigma^{70}$  including facilitating transcriptional elongation (Kapanidis et al., 2005; Goldman et al., 2015; Perdue and Roberts, 2011; Mooney and Landick, 2003; Mooney et al., 2005). **Figure 7** (B) is suggestive of such a role as the number of  $\sigma^{70}$  proteins per cell is in close agreement with our estimate of the number of transcriptional complexes needed.

These estimates provide insight as to the observed magnitude of both RNA polymerase and the  $\sigma$ -70 factor. As we have done in the previous sections, and described in the supplemental information, we can generalize these estimates across a wide range of growth rates (grey line in **Figure 7(B)**). While there remains some disagreement in the magnitude of the copy number, this estimate appears to very adequately describe the growth rate dependence of these complexes. Furthermore, these findings illustrate that transcription cannot be the rate limiting step in bacterial division. **Figure 7** (A) reveals that the availability of RNA polymerase is not a limiting factor for cell division as the cell always has an apparent  $\sim$  10-fold excess than needed. Furthermore, if more transcriptional activity was needed to satisfy the cellular requirements, more  $\sigma^{70}$ -factors could be expressed to utilize a larger fraction of the RNA polymerase pool.

### 539 Translation and Ribosomal Synthesis

540 Lastly, we turn our attention to the process of synthesizing new proteins, translation. This process  
 541 stands as a good candidate for potentially limiting growth since the synthesis of new proteins relies  
 542 on the generation of ribosomes, themselves proteinaceous molecules. As we will see in the coming  
 543 sections of this work, this poses a "chicken-or-the-egg" problem where the synthesis of ribosomes  
 544 requires ribosomes in the first place.

545 We will begin our exploration of protein translation in the same spirit as we have in previous sections – we will draw order-of-magnitude estimates based on our intuition and available literature,  
 546 and then compare these estimates to the observed data. In doing so, we will estimate both the  
 547 absolute number of ribosomes necessary for replication of the proteome as well as the synthesis  
 548 of amino-acyl tRNAs. From there we consider the limitations on ribosomal synthesis in light of our  
 549 estimates on both the synthesis of ribosomal proteins and our earlier results on rRNA synthesis.

#### 551 tRNA Synthetases

552 We begin by first estimating the number of tRNA synthetases in *E. coli* needed to convert free amino-  
 553 acids to polypeptide chains. At a modest growth rate of  $\approx$  5000 s, *E. coli* has roughly  $3 \times 10^6$  proteins  
 554 per cell (BNID: 115702; Milo et al. (2010)). Assuming that the typical protein is on the order of  $\approx$   
 555 300 amino acids in length (BNID: 100017; Milo et al. (2010)), we can estimate that a total of  $\approx 10^9$   
 556 amino acids are stitched together by peptide bonds.

557 How many tRNAs are needed to facilitate this remarkable number of amino acid delivery events  
 558 to the translating ribosomes? It is important to note that tRNAs are recycled after they've passed  
 559 through the ribosome and can be recharged with a new amino acid, ready for another round of  
 560 peptide bond formation. While some *in vitro* data exists on the turnover of tRNA in *E. coli* for  
 561 different amino acids, we can make a reasonable estimate by comparing the number of amino  
 562 acids to be polymerized to cell division time. Using our stopwatch of 5000 s and  $10^9$  amino acids,  
 563 we arrive at a requirement of  $\approx 2 \times 10^5$  tRNA molecules to be consumed by the ribosome per  
 564 second.

565 There are many processes which go into synthesizing a tRNA and ligating it with the appropriate  
 566 amino acids. As we discussed previously, there appear to be more than enough RNA polymerases  
 567 per cell to synthesize the needed pool of tRNAs. Without considering the many ways in which  
 568 amino acids can be scavenged or synthesized *de novo*, we can explore ligation the as a potential  
 569 rate limiting step. The enzymes which link the correct amino acid to the tRNA, known as tRNA  
 570 synthetases or tRNA ligases, are incredible in their proofreading of substrates with the incorrect  
 571 amino acid being ligated once out of every  $10^4$  to  $10^5$  times (BNID: 103469, Milo et al. (2010)). This  
 572 is due in part to the consumption of energy as well as a multi-step pathway to ligation. While the

573 rate at which tRNA is ligated is highly dependent on the identity of the amino acid, it is reasonable  
 574 to state that the typical tRNA synthetase has charging rate of  $\approx 20$  AA per tRNA synthetase per  
 575 second (BNID: 105279, *Milo et al. (2010)*).

576 We can make an assumption that amino-acyl tRNAs are in steady-state where they are pro-  
 577 duced at the same rate they are consumed, meaning that  $2 \times 10^5$  tRNAs must be charged per sec-  
 578 ond. Combining these estimates together, as shown schematically in *Figure 8(A)*, yields an estimate  
 579 of  $\approx 10^4$  tRNA synthetases per cell with a division time of 5000 s. This point estimate is in very close  
 580 agreement with the observed number of synthetases (the sum of all 20 tRNA synthetases in *E. coli*).  
 581 This estimation strategy seems to adequately describe the observed growth rate dependence of  
 582 the tRNA synthetase copy number (shown as the grey line in *Figure 8(B)*), suggesting that the copy  
 583 number scales with the cell volume.

584 In total, the estimated and observed  $\approx 10^4$  tRNA synthetases occupy only a meager fraction of  
 585 the total cell proteome, around 0.5% by abundance. It is reasonable to assume that if tRNA charg-  
 586 ing was a rate limiting process, cells would be able to increase their growth rate by devoting more  
 587 cellular resources to making more tRNA synthases. As the synthesis of tRNAs and the correspond-  
 588 ing charging can be highly parallelized, we can argue that tRNA charging is not a rate limiting step  
 589 in cell division, at least for the growth conditions explored in this work.

#### 590 Protein Synthesis

591 With the number of tRNA synthetases accounted for, we now consider the abundance of the pro-  
 592 tein synthesis machines themselves, ribosomes. Ribosomes are enormous protein/rRNA com-  
 593 plexes that facilitate the peptide bond formation between amino acids in the correct sequence  
 594 as defined by the coding mRNA. Before we examine the synthesis of the ribosome proteins and  
 595 the limits that may place on the observed bacterial growth rates, let's consider replication of the  
 596 cellular proteome.

597 As described in the previous section, an *E. coli* cell consisting of  $\approx 3 \times 10^6$  proteins will have  
 598 on the order  $\approx 10^9$  peptide bonds per proteome. While the rate at which ribosomes translates is  
 599 well known to have a growth rate dependence *Dai et al. (2018)* and is a topic which we discuss in  
 600 detail in the coming sections. However, for the purposes of our order-of-magnitude estimate, we  
 601 can make the approximation that translation occurs at a rate of  $\approx 15$  amino acids per second per  
 602 ribosome (BNID: 100233, *Milo et al. (2010)*). Under this approximation and assuming a division  
 603 time of 5000 s, we can arrive at an estimate of  $\approx 10^4$  ribosomes are needed to replicate the cellular  
 604 proteome, shown in *Figure 8(B)*. This point estimate, while glossing over important details such  
 605 as chromosome copy number and growth-rate dependent translation rates, proves to be notably  
 606 accurate when compared to the experimental observations (*Figure 8(B)*).

#### 607 Translation as a Growth-Rate Limiting Step

608 Thus far, the general back-of-the-envelope estimates have been reasonably successful in explain-  
 609 ing what sets the scale of absolute protein copy number. A recurring theme that has arisen is the  
 610 ability of cells to parallelize their biosynthesis tasks. For example, while DNA replication speed-limit  
 611 is  $\approx 40$  minutes to replicate a genome, cells can divide faster than this by initiating more than one  
 612 round of replication per doubling. However, as we will see, parallelization is not possible when it  
 613 comes to the translation of ribosomal proteins (*Figure 9(A)*). Thus, it is plausible that translation  
 614 may be a key factor in determining the cellular growth rate.

615 To gain some intuition into how translation can set the speed of bacterial growth, we again  
 616 consider the total number of peptide bonds that must be synthesized, which we denote as  $N_{AA}$ .  
 617 Noting that cells grow exponentially in time (*Godin et al., 2010*), we can compute the number of  
 618 amino acids to be polymerized as

$$N_{AA} \lambda = r_i R, \quad (1)$$

619 where  $\lambda$  is the cell growth rate in  $s^{-1}$ ,  $r_i$  is the maximum translation rate in  $AA \cdot s^{-1}$ , and  $R$  is the  
 620 average ribosome copy number per cell. Knowing the number of peptide bonds to be formed

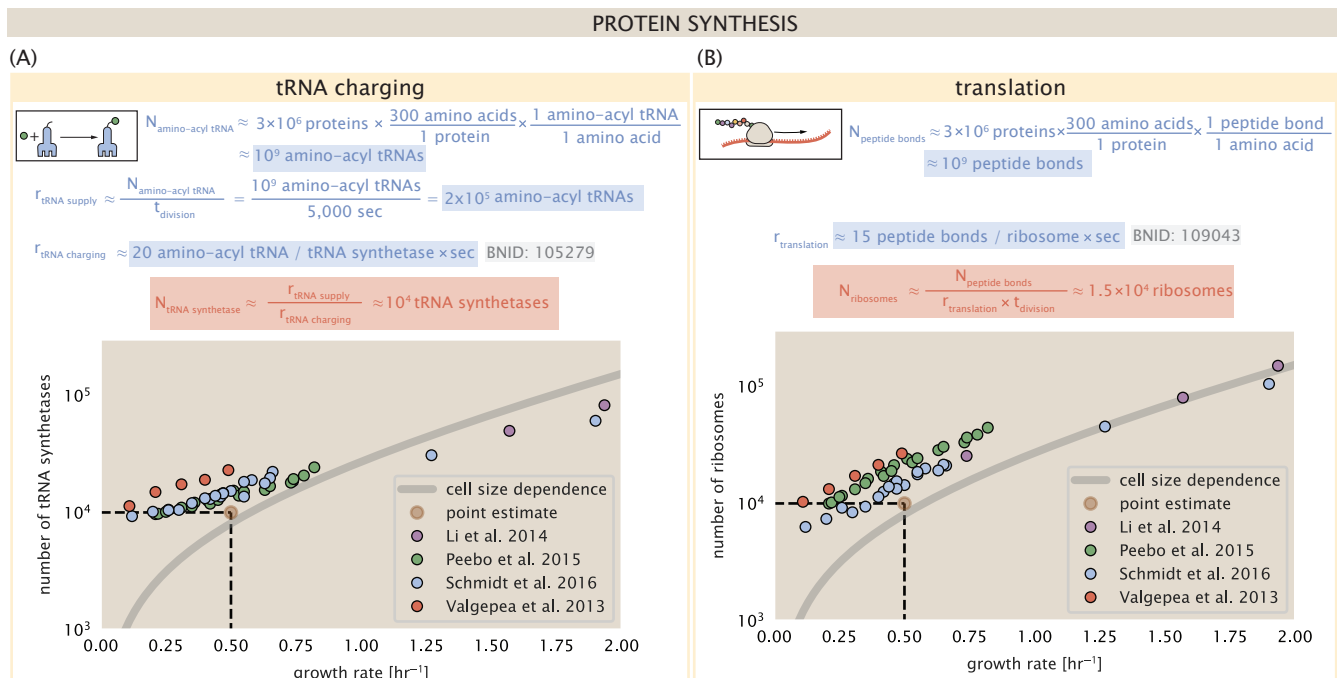


**Figure 8. Estimation of the required tRNA synthetases and ribosomes.** (A) Estimation for the number of tRNA synthetases that will supply the required amino acid demand. The sum of all tRNA synthetases copy numbers are plotted as a function of growth rate ([ArgS], [CysS], [GlnS], [Glx], [IleS], [LeuS], [ValS], [AlaS]<sub>2</sub>, [AsnS]<sub>2</sub>, [AspS]<sub>2</sub>, [TyrS]<sub>2</sub>, [TrpS]<sub>2</sub>, [ThrS]<sub>2</sub>, [SerS]<sub>2</sub>, [ProS]<sub>2</sub>, [PheS]<sub>2</sub>[PheT]<sub>2</sub>, [MetG]<sub>2</sub>, [LysS]<sub>2</sub>, [HisS]<sub>2</sub>, [GlyS]<sub>2</sub>[GlyQ]<sub>2</sub>). (B) Estimation of the number of ribosomes required to synthesize 10<sup>9</sup> peptide bonds with an elongation rate of 15 peptide bonds per second. The average abundance of ribosomes is plotted as a function of growth rate. Our estimated values are shown for a growth rate of 0.5 hr<sup>-1</sup>. Grey lines correspond to the estimated complex abundance calculated at different growth rates. See Supplemental Information XX for a more detail description of this calculation.

621 permits us to compute the translation-limited growth rate as

$$\lambda_{\text{translation-limited}} = \frac{r_t R}{N_{\text{AA}}}. \quad (2)$$

622 Alternatively, since  $N_{\text{AA}}$  is related to the total protein mass through the molecular weight of  
 623 each protein, we can also consider the growth rate in terms of the fraction of the total proteome  
 624 mass that is dedicated to ribosomal protein mass. By making the approximation that an average  
 625 amino acid has a molecular weight of 110 Da (BNID: 104877, *Milo et al. (2010)*), we can approximate  
 626  $R/N_{\text{AA}} \approx \Phi_R/L_R$ , where  $\Phi_R$  is the ribosomal mass fraction and  $L_R$  is the total length in amino acids  
 627 that make up a ribosome. The translation-limited growth rate can then be written in the form

$$\lambda_{\text{translation-limited}} \approx \frac{r_t}{L_R} \Phi_R. \quad (3)$$

628 This is plotted as a function of ribosomal fraction  $\Phi_R$  in *Figure 9(B)*, where we take  $L_R \approx 7500$  AA,  
 629 corresponding to the length in amino acids for all ribosomal subunits of the 50S and 30S complex  
 630 (BNID: 101175, *(Milo et al., 2010)*).

631 The growth rate defined by *Equation 3* reflects mass-balance under steady-state growth and  
 632 has long provided a rationalization of the apparent linear increase in *E. coli*'s ribosomal content  
 633 as a function of growth rate (*Maaløe, 1979; Scott et al., 2010*). We note that there is a maximum  
 634 growth rate of  $\lambda \approx 8 \text{ hr}^{-1}$ , or a doubling time just under 6 minutes (*Figure 9(B)*, dashed line). This  
 635 represents an inherent speed limit due to the need for the cell to double its entire ribosomal mass.  
 636 Interestingly, this limit is independent of the absolute number of ribosomes and is simply given by  
 637 the time to translate an entire ribosome,  $L_R/r_t$ . As shown in *Figure 9(A)*, we can reconcile this with  
 638 the observation that in order to double the average number of ribosomes, each ribosome must  
 639 produce a second ribosome and cannot be parallelized.

640 Earlier, we considered rRNA synthesis (see Section **RNA Synthesis**), finding that, when the rRNA  
 641 operons are maximally loaded with RNA polymerase, the cell can produce  $\approx 1$  functional rRNA unit  
 642 per second per operon. In *Figure 9(C)*, we show the maximum number of ribosomes that could  
 643 be made as a function of growth rate given this rRNA production rule-of-thumb. While each *E.*  
 644 *coli* genome has 7 copies of the rRNA operon (BNID: 107866, *Milo et al. (2010)*), parallelization  
 645 of DNA synthesis by firing multiple rounds of replication at a time can drastically the effective  
 646 number of rRNA operons. The blue curve in *Figure 9(C)*, we assume that the effective number of  
 647 rRNA operons increases in proportion to the number of origins of replication  $\langle \# \text{ ori} \rangle$  (solid blue  
 648 line; with the calculation of  $\langle \# \text{ ori} \rangle$  described in the next section). Although we expect this value to  
 649 drastically overestimate rRNA abundance at slower growth rates ( $\lambda < 0.5 \text{ hr}^{-1}$ ), it provides a useful  
 650 reference when considered along with the proteomic measurements that are also plotted. For  
 651 growth rates above about  $1 \text{ hr}^{-1}$ , we find that cells will need to transcribe rRNA near their maximal  
 652 rate. The dashed blue curve in *Figure 9(C)* shows the maximal number of functional rRNA units  
 653 that could be synthesized from a single genome (ignoring the chromosome replication speed limit  
 654 of  $\approx 40$  minutes per genome). The convergence between the maximum rRNA production with  
 655 parallelization and the experimentally measured ribosome copy number (points in *Figure 9(C)*), as  
 656 well as the observation cells are rarely reported to grow faster than  $2 \text{ hr}^{-1}$  (*Bremer and Dennis,*  
 657 *2008*), suggests rRNA synthesis represents the rate limiting step in cell division for this strain of *E.*  
 658 *coli*.

### 659 Relationship Between Cell Size and Growth Rate

660 With the observation that ribosomes set an inherent upper limit on growth rate, through both rRNA  
 661 synthesis and the additional dependence on ribosomal fraction, it is also plausible that ribosomes  
 662 may play a more dominant role in setting growth rate across other growth conditions. With a rich  
 663 proteomic data set across a wide array of conditions, and in light of a number of recent experi-  
 664 mental observations, we find that cells also appear to tune their ribosomal abundance as a means  
 665 to maximize growth even in poor nutrient conditions. This has important consequences on the

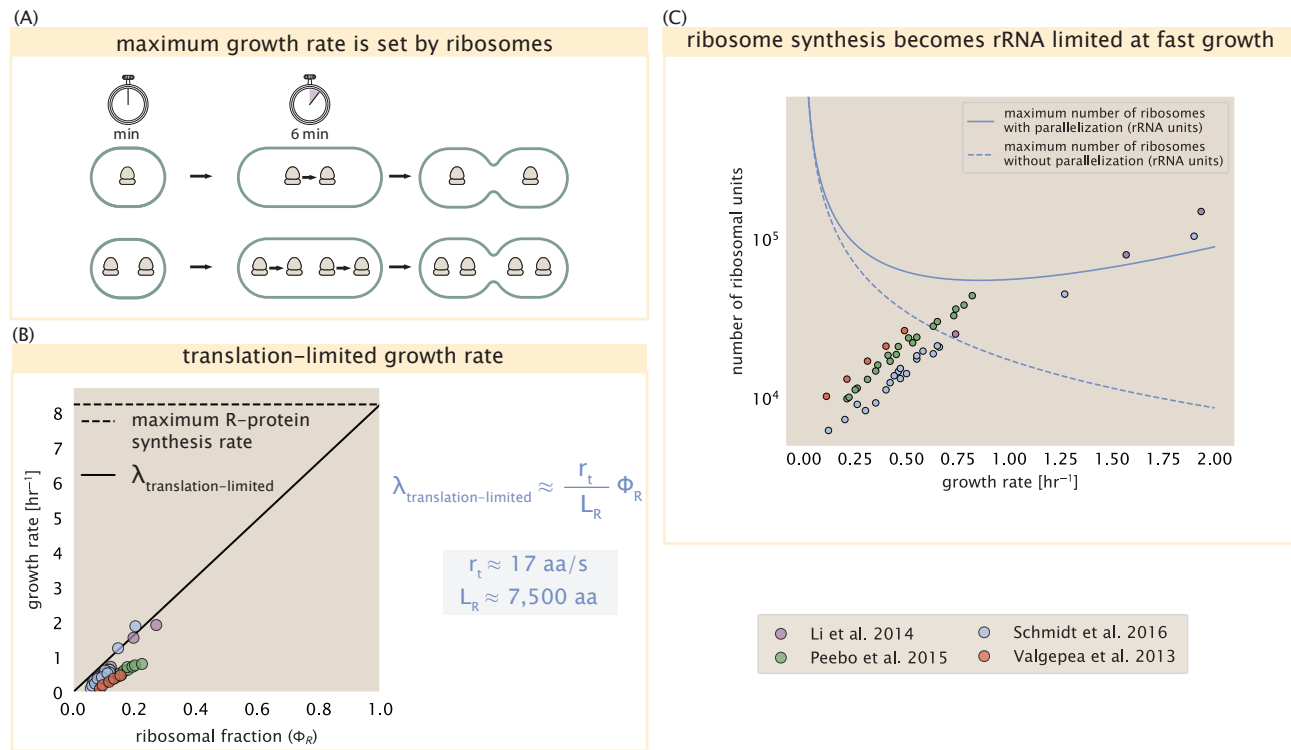


**Figure 9. Translation-limited growth rate.** (A) Here we consider the translation-limited growth rate as a function of ribosomal fraction. By mass balance, the time required to double the entire proteome ( $N_{AA} / r_t$ ) sets the translation-limited growth rate,  $\lambda_{\text{translation-limited}}$ . Here  $N_{AA}$  is effectively the number of peptide bonds that must be translated,  $r_t$  is the translation elongation rate, and  $R$  is the number of ribosomes. This can also be re-written in terms of the ribosomal mass fraction  $\Phi_R = m_R / m_{\text{protein}}$ , where  $m_R$  is the total ribosomal mass and  $m_{\text{protein}}$  is the mass of all proteins in the cell.  $L_R$  refers to the summed length of the ribosome in amino acids.  $\lambda_{\text{translation-limited}}$  is plotted as a function of  $\Phi_R$  (solid line). (B) The dashed line in part (A) identifies a maximum growth rate that is set by the ribosome. Specifically, this growth rate corresponds to the time required to translate an entire ribosome,  $L_R / r_t$ . This is a result that is independent of the number of ribosomes in the cell as shown schematically here. (C) Maximum number of rRNA units that can be synthesized as a function of growth rate. Solid curve corresponds to the rRNA copy number calculated by multiplying the number of rRNA operons by the estimated number of (# ori) at each growth rate. The quantity (# ori) was calculated using Equation 4 and the measurements from Si et al. (2017) that are plotted in Figure 10(A). Dashed line show that maximal number of functional rRNA units produced from a single chromosome without parallelization.

666 relationship with cell size and maintenance of steady-state growth. In the coming section and the  
667 remainder of the text, we consider these further beginning with cell size.

668 The relationship between cell size and growth rate has long been of interest in the study of  
669 bacterial physiology, particularly following the now six decade-old observation that cell volume  
670 appears to increase exponentially with growth rate; known as Schaechter's growth law (*Schaechter*  
671 *et al.*, 1958; *Taheri-Araghi et al.*, 2015). Wild-type *E. coli* growing at relatively fast growth rates  
672 exhibit a remarkably constant cell cycle time  $t_{cyc}$  (referring to the C and D periods of DNA replication  
673 and cell division, respectively), as shown in **Figure 10(A)** for the data reproduced from *Si et al.* (2017).  
674 With a constant cell cycle time, the exponential scaling in size has long been considered a direct  
675 consequence of cells initiating replication at a constant volume per origin. However, the particular  
676 mechanism that governs this relationship, and even the question of whether the change in average  
677 cell size is truly exponential have remained under debate (*Si et al.*, 2017; *Harris and Theriot*, 2018).

678 Since protein accounts for more than half of cellular dry mass (BNID: 104954, *Milo et al.* (2010);  
679 *Bremer and Dennis* (2008); *Basan et al.* (2015), cell size will vary in proportion to how much protein  
680 is synthesized over the cell cycle. Through our estimates in the sections on the central dogma, it is  
681 apparent that the processes of transcription (i.e. synthesis of mRNA) and translation are unlikely  
682 limiting steps in doubling the cell mass. In both cases, there is an overabundance of the requisite  
683 protein complexes (DNA and RNA polymerase, respectively) and there are mechanisms by which  
684 these synthesis processes can be parallelized. Therefore, the total protein mass is determined by  
685  $r_i \times R$  and the doubling time  $\tau$ . The relationship between cell size and growth rate, however, will  
686 depend only on how the cell scales its ribosomal fraction  $\Phi_R$ , as highlighted by **Equation 3**.

#### 687 Exponential Scaling of Cell Size Follows from a Need to Increase Absolute Ribosomal 688 Abundance.

689 A naïve strategy to increase growth rate given the constraint prescribed by **Equation 3**, would be  
690 to simply generate more ribosomes. In reality, large swaths of the proteome increases in absolute  
691 abundance at faster growth (Supplemental Figure X). Substantial empirical evidence has revealed  
692 a linear scaling between cell size (volume) and the number of chromosomal origins of replication,  
693  $\langle \# \text{ ori} \rangle$ , which is robust to a remarkable array of perturbations (*Si et al.*, 2017). The number of  
694 origins  $\langle \# \text{ ori} \rangle$  is determined by how often replication must be initiated per cell doubling to maintain  
695 steady-state growth and can be quantified via

$$\langle \# \text{ ori} \rangle \approx 2^{t_{cyc}/\tau}, \quad (4)$$

696 where  $\tau$  is the doubling time. In **Figure 10(A)**, we show the measurements of *Si et al.* (2017) for  
697 wild-type *E. coli* cells in nutrient-limit growth regimes. Using this data, we estimated  $\langle \# \text{ ori} \rangle$  for each  
698 condition in the amalgamated proteomic datasets. With rRNA otherwise becoming rate limited at  
699 fast growth, this strategy allows for a roughly linear increase in ribosomes copy number with  $\langle \#$   
700  $\text{ori} \rangle$  as shown in **Figure 10(B)** for the proteomic data.

701 It is notable that in *E. coli*, the majority of ribosomal proteins and rRNA operons are found  
702 closer to the origin of replication. Since multiple rounds of DNA initiation will effectively skew gene  
703 dosage in favor of genes near the origin (*Scholz et al.*, 2019), it suggests that an increase in  $\langle \# \text{ ori} \rangle$   
704 is a means to skew the ribosomal fraction of the proteome,  $\Phi_R$ . In **Figure 10(D)** we show that this  
705 skew in gene dosage is reflected in the composition of the proteome via a running boxcar average  
706 (500 kbp window) of protein copy number as a function of each gene's transcriptional start site  
707 (**Figure 10(D)**). While the protein copy numbers of individual proteins can vary substantially across  
708 the entire chromosome, we nonetheless observe a bias in expression across the chromosome  
709 under fast growth conditions (dark blue lines) relative to slow growth (yellow lines). The dramatic  
710 change in protein copy number near the origin is largely due to the increase in ribosomal protein  
711 expression. This trend is in contrast to slower growth conditions (yellow) where the average copy  
712 number is much more uniform across the length of the chromosome.

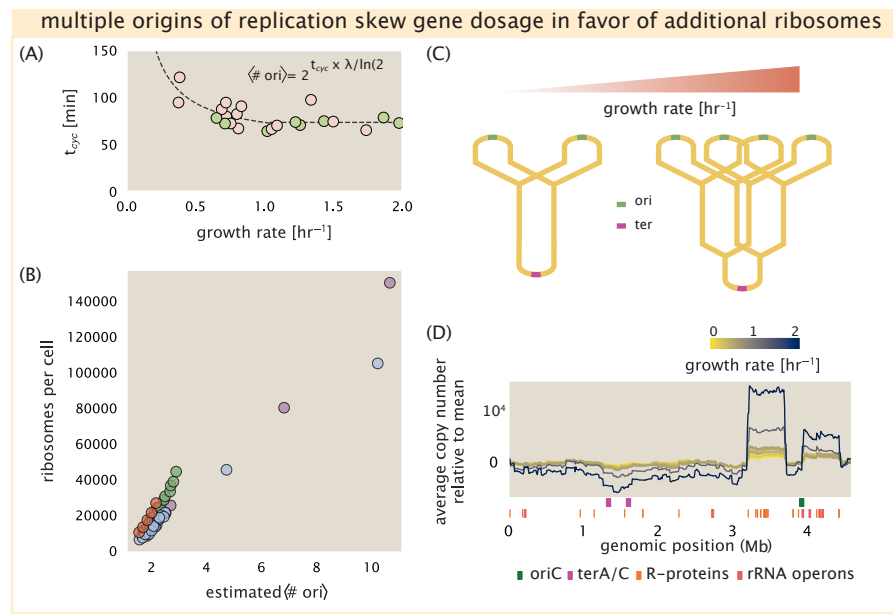


**Figure 10. Multiple replication forks skew gene dosage and ribosomal content.** (A) Experimental data from Si *et al.* (2017). Dashed line shows fit to the data, which were used to estimate  $\langle \# \text{ori} \rangle$ .  $t_{\text{cyc}}$  was assumed to vary in proportion to  $\tau$  for doubling times great than 40 minutes, and then reach a minimum value of [fill in] minutes below this (see Supplemental Appendix X for additional details). Red data points correspond to measurements in strain MG1655, while light green points are for strain NCM3722. (B) Plot of the ribosome copy number estimated from the proteomic data against the estimated  $\langle \# \text{ori} \rangle$  [NB: change to total protein abundance?]. (C) Schematic shows the expected increase in replication forks (or number of ori regions) as *E. coli* cells grow faster. (D) A running boxcar average of protein copy number is calculated for each each growth condition considered by (Schmidt *et al.*, 2016). A 0.5 Mb averaging window was used. Protein copy numbers are reported relative to their condition-specific means in order to center all data sets.

713 This result provides important evidence that although total protein content scales with  $\langle \# \text{ ori} \rangle$ , it  
 714 is also the bias in gene dosage for genes closer to the origin that change the proteomic composition  
 715 and allows an increase in the ribosomal fraction  $\Phi_R$  at fast growth. For *E. coli*, we can then view  
 716 the increase in ribosomal fraction  $\Phi_R$  (and therefore,  $\lambda$ ) as requiring a geometric increase in total  
 717 protein abundance that is proportional to  $\langle \# \text{ ori} \rangle$ . This leads to an exponential increase in total  
 718 protein mass (and cell size) as long as all ribosomes  $R$  are actively translating protein during cell  
 719 doubling.

720 While our analysis suggests that it is the need to increase the absolute number of ribosomes  
 721 that sets an exponential scaling in cell size, this relationship is likely to falter at slow growth rates  
 722 (below  $\lambda \approx 0.5 \text{ hr}^{-1}$ ). In this regime, ribosome abundance  $R$  no longer reflects the cell's protein syn-  
 723 thesis capacity (*Dai et al., 2016*), so far taken to be  $r_t \times R$ . Additional regulatory control through the  
 724 small-molecule alarmones such as guanosine pentaphosphate [(p)ppGpp] reduces the fraction of  
 725 actively translating ribosomes at slow growth and yields a translational capacity below  $r_t \times R$ . This  
 726 is why *Si et al. (2017)* found that it was the change in active ribosomal fraction, and not riboso-  
 727 mal fraction alone, that was most consistent with an exponential change in cell size. The specific  
 728 relationship between cell size and growth rate however becomes harder to define because cells  
 729 no longer need multiple rounds of DNA replication to make enough rRNA, and no longer need to  
 730 increase their total protein mass in order to tune protein synthesis. Our collated proteomic data,  
 731 however, contain several assumptions that relate total protein abundance to growth rates and this  
 732 prevents us from making precise predictions about how cell size and absolute protein abundance  
 733 vary at slow growth (Supplemental X). Nevertheless, we find no evidence that cells decrease their  
 734 size to the minimal value expected from on an exponential function with a constant exponent fit  
 735 to cell sizes with moderate to fast growth rates (*Basan et al., 2015; JL et al., 2016; Si et al., 2019*),  
 736 suggesting at least a modified scaling between size and growth rate in these poorer nutrient con-  
 737 ditions.

### 738 Growth in Poor Nutrient Conditions.

739 How do cells regulate protein synthesis when amino acids become limiting, meaning that con-  
 740 sumption exceeds the rate of synthesis? In the slowest growth conditions, we find a minimum  
 741 ribosomal mass fraction of  $\Phi_R \approx 0.06$  and of order  $10^4$  ribosomes per cell. Without the additional  
 742 regulatory control noted above, there would be a point where this imbalance would occur if all  
 743 ribosomes were actively translating (*Figure 11*). Such a scenario would prevent continuous growth,  
 744 and indeed for (p)ppGpp null strains, cells only grow in minimal media if additional amino acid  
 745 supplements are present. In contrast, wild-type *E. coli* maintain a relatively high elongation rate  
 746 even in stationary phase ( $\approx 8 \text{ AA/s}$ , (*Dai et al., 2016, 2018*)).

747 To better understand how regulation of ribosomes influence growth rate at slow growth, we  
 748 consider a coarse-grained model that relates elongation rate to a limiting supply of amino acids,  
 749 which for simplicity we treat as a single, effective rate-limiting species  $[AA]_{eff}$ . Under such a sce-  
 750 nario, the elongation rate  $r_t$  can be described as depending on the maximum elongation rate ( $r_t^{max} \approx$   
 751  $17.1 \text{ AA/s}$ , (*Dai et al., 2016, 2018*)), an effective binding constant  $K_D$  between the pool of amino acids  
 752 and their amino-acyl tRNAs, and the limiting amino acid concentration  $[AA]_{eff}$ ,

$$r_t = r_t^{max} \cdot \frac{1}{1 + K_D/[AA]_{eff}}. \quad (5)$$

753 For cells growing in minimal medium supplemented with glucose, the amino acid concentration is  
 754 of order 100 mM (BNID: 110093, (*Milo et al., 2010; Bennett et al., 2009*)). To estimate  $K_D$ , we note  
 755 that for a growth rate of about  $0.6 \text{ hr}^{-1}$  *Dai et al. (2016)* measured an elongation rate of about  $12.5$   
 756  $\text{AA} \cdot \text{s}^{-1}$ , yielding  $K_D \approx 40 \text{ mM}$ . The maintenance of this amino acid pool  $[AA]_{eff}$  will depend on the  
 757 difference between the synthesis/supply rate of amino acids  $r_{AA}$  and consumption by ribosomes  
 758  $r_t \times R \times f_a$ , where we use  $f_a$  to account for the possible reduction of actively translating ribosomes  
 759 (see Supplemental Appendix XX for further details on this model).

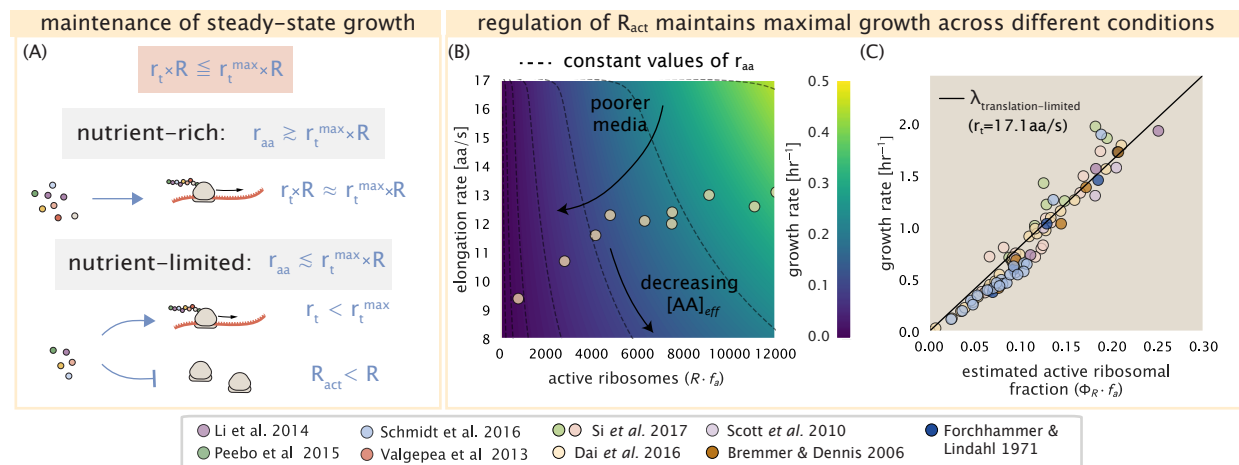


**Figure 11. *E. coli* must regulate ribosomal activity in limiting nutrient conditions.** (A) Schematic showing translation-specific requirements for maintenance of steady-state growth. In a nutrient rich environment, amino acid supply  $r_{aa}$  is sufficiently in excess of the demand by ribosomes translating at their maximal rate. In poorer nutrient conditions, reduced amino acid supply  $r_{aa}$  will decrease the rate of elongation. In a regime where  $r_{aa}$  is less than  $r_t R$ , the number of actively translating ribosomes will need to be reduced in order to maintain steady-state growth. (B) Translation elongation rate is plotted as a function of the number of actively translating ribosomes  $R f_a$ . Dashed lines correspond to a range of amino acid synthesis rates  $r_{aa}$ , from  $10^3$  to  $10^6$ . Growth rates are calculated according to Equation 1, assuming a constant ribosomal fraction of 8 percent. See appendix XX for additional details. (C) Experimental data from (Dai et al., 2016) are used to estimate the fraction of actively translating ribosomes. The solid line represents the translation-limited growth rate for ribosomes elongating at 17.1 AA/s.

760     In **Figure 11(B)**, we show the relationship between the growth rate and elongation rate as a  
 761     function of the number of actively translating ribosomes. Here, growth rate is now determined by  
 762     the active ribosomal fraction via

$$\lambda_{\text{translation-limited}} \approx \frac{r_t}{L_R} \Phi_R f_a. \quad (6)$$

763     If we consider constant values of amino acid synthesis rate  $r_{AA}$  (dashed lines) to reflect the available  
 764     parameter space for a specific growth condition, the fastest growth rates result from maximization  
 765     of the fraction of actively translating ribosomes. When we consider the experimental measure-  
 766     ments from **Dai et al. (2018)** (yellow circles), reflecting growth in different nutrient conditions, we  
 767     see that although  $R \times f_a$  is reduced in poorer nutrient conditions, it is reduced in a manner such that  
 768      $[AA]_{eff}$  is relatively constant. Given our estimate  $K_D \approx 40 \text{ mM}$ , we would only expect a decrease  
 769     from 100 mM to about 35 mM in the slowest growth conditions. While experimental data is scarce,  
 770     data from **Bennett et al. (2009)** show that amino acid concentrations only decrease to about 60  
 771     mM for cells grown in minimal media supplemented with acetate ( $\lambda \approx 0.3 \text{ hr}^{-1}$  in our proteomic  
 772     data) (**Bennett et al., 2009**), qualitatively consistent with our expectations. One explanation for the  
 773     experimental data is that the active fraction of the ribosome pool is regulated in order to maintain  
 774     a sufficient supply of amino acids for growth. Any further increase in  $R \times f_a$  at constant  $r_{AA}$  would  
 775     otherwise be associated with an additional drop in cellular amino acid concentration.

#### 776     ***E. coli* Maximizes its Steady-State Growth Rate by Tuning both Ribosomal Content and 777     Translation Activity.**

778     Using the active fraction  $f_a$  measurements across a broad range of nutrient-limited growth condi-  
 779     tions from the work of **Dai et al. (2016)**, we furthermore estimated the active fraction of ribosomal  
 780     protein across the collated proteomic datasets (**Figure 11(C)**). Importantly, we note that across all  
 781     growth conditions considered, cells appear to maintain a growth rate consistent with **Equation 3**  
 782     with an elongation rate of  $r_t \approx 17.1 \text{ AA/s}$ . While somewhat counter intuitive, given that ribosomes

783 translate at almost half this rate in the poorest of growth conditions, steady-state growth rates can  
784 be achieved over such a broad range of conditions because cells have evolved a means to tune  
785  $r_t \times R \times f_a$ .

786 It has recently been shown that growth in a (p)ppGpp null strain abolishes both the the growth-  
787 dependent changes in gene dosage and scaling in cell size. Instead, cells always exhibited a higher  
788 gene dosage near near the origin of replication, irrespective of growth rate, and a cell size more  
789 consistent with a fast growth state where (p)ppGpp levels are low (*Fernández-Coll et al., 2020*) and  
790 ribosomal fraction is high (*Zhu and Dai, 2019*). This raises the possibility that the action of (p)ppGpp  
791 is also mediating growth control and size scaling over the entire range of growth conditions. Specif-  
792 ically, as nutrient conditions worsen, (p)ppGpp helps decrease multiple rounds of DNA replication  
793 per cell doubling which effectively decreases both  $R$  and the total cell size *and* in sufficiently poor  
794 growth conditions mitigates translation activity according to nutrient availability.

## 795      References

- 796      Abelson, H., Johnson, L., Penman, S., and Green, H. (1974). Changes in RNA in relation to growth of the fibroblast:  
 797      II. The lifetime of mRNA, rRNA, and tRNA in resting and growing cells. *Cell*, 1(4):161–165.
- 798      Aidelberg, G., Towbin, B. D., Rothschild, D., Dekel, E., Bren, A., and Alon, U. (2014). Hierarchy of non-glucose  
 799      sugars in *Escherichia coli*. *BMC Systems Biology*, 8(1):133.
- 800      Antonenko, Y. N., Pohl, P., and Denisov, G. A. (1997). Permeation of ammonia across bilayer lipid membranes  
 801      studied by ammonium ion selective microelectrodes. *Biophysical Journal*, 72(5):2187–2195.
- 802      Ashburner, M., Ball, C. A., Blake, J. A., Botstein, D., Butler, H., Cherry, J. M., Davis, A. P., Dolinski, K., Dwight, S. S.,  
 803      Eppig, J. T., Harris, M. A., Hill, D. P., Issel-Tarver, L., Kasarskis, A., Lewis, S., Matese, J. C., Richardson, J. E.,  
 804      Ringwald, M., Rubin, G. M., and Sherlock, G. (2000). Gene Ontology: tool for the unification of biology. *Nature Genetics*, 25(1):25–29.
- 805      Ason, B., Bertram, J. G., Hingorani, M. M., Beechem, J. M., O'Donnell, M., Goodman, M. F., and Bloom, L. B.  
 806      (2000). A Model for *Escherichia coli* DNA Polymerase III Holoenzyme Assembly at Primer/Template Ends:  
 807      DNA Triggers A Change In Binding Specificity of the  $\gamma$  Complex Clamp Loader. *Journal of Biological Chemistry*,  
 808      275(4):3006–3015.
- 809      Assentoft, M., Kaptan, S., Schneider, H.-P., Deitmer, J. W., de Groot, B. L., and MacAulay, N. (2016). Aquaporin 4  
 810      as a NH<sub>3</sub> Channel. *Journal of Biological Chemistry*, 291(36):19184–19195.
- 811      Basan, M., Zhu, M., Dai, X., Warren, M., Sévin, D., Wang, Y.-P., and Hwa, T. (2015). Inflating bacterial cells by  
 812      increased protein synthesis. *Molecular Systems Biology*, 11(10):836.
- 813      Bauer, S. and Ziv, E. (1976). Dense growth of aerobic bacteria in a bench-scale fermentor. *Biotechnology and  
 814      Bioengineering*, 18(1):81–94. \_eprint: <https://onlinelibrary.wiley.com/doi/pdf/10.1002/bit.260180107>.
- 815      Belliveau, N. M., Barnes, S. L., Ireland, W. T., Jones, D. L., Sweredoski, M. J., Moradian, A., Hess, S., Kinney, J. B.,  
 816      and Phillips, R. (2018). Systematic approach for dissecting the molecular mechanisms of transcriptional  
 817      regulation in bacteria. *Proceedings of the National Academy of Sciences*, 115(21):E4796–E4805.
- 818      Bennett, B. D., Kimball, E. H., Gao, M., Osterhout, R., Van Dien, S. J., and Rabinowitz, J. D. (2009). Absolute  
 819      metabolite concentrations and implied enzyme active site occupancy in *Escherichia coli*. *Nature Chemical  
 820      Biology*, 5(8):593–599.
- 821      Birnbaum, L. S. and Kaplan, S. (1971). Localization of a Portion of the Ribosomal RNA Genes in *Escherichia coli*.  
 822      *Proceedings of the National Academy of Sciences*, 68(5):925–929.
- 823      Booth, I. R., Mitchell, W. J., and Hamilton, W. A. (1979). Quantitative analysis of proton-linked transport systems.  
 824      The lactose permease of *Escherichia coli*. *Biochemical Journal*, 182(3):687–696.
- 825      Bremer, H. and Dennis, P. P. (2008). Modulation of Chemical Composition and Other Parameters of the Cell at  
 826      Different Exponential Growth Rates. *EcoSal Plus*, 3(1).
- 827      Browning, D. F. and Busby, S. J. W. (2016). Local and global regulation of transcription initiation in bacteria.  
 828      *Nature Reviews Microbiology*, 14(10):638–650.
- 829      Cox, G. B., Newton, N. A., Gibson, F., Snoswell, A. M., and Hamilton, J. A. (1970). The function of ubiquinone in  
 830      *Escherichia coli*. *Biochemical Journal*, 117(3):551–562.
- 831      Dai, X., Zhu, M., Warren, M., Balakrishnan, R., Okano, H., Williamson, J. R., Fredrick, K., and Hwa, T. (2018).  
 832      Slowdown of Translational Elongation in *Escherichia coli* under Hyperosmotic Stress. - PubMed - NCBI. *mBio*,  
 833      9(1):281.
- 834      Dai, X., Zhu, M., Warren, M., Balakrishnan, R., Patsalo, V., Okano, H., Williamson, J. R., Fredrick, K., Wang, Y.-P.,  
 835      and Hwa, T. (2016). Reduction of translating ribosomes enables *Escherichia coli* to maintain elongation rates  
 836      during slow growth. *Nature Microbiology*, 2(2):16231.
- 837      Escalante, A., Salinas Cervantes, A., Gosset, G., and Bolívar, F. (2012). Current knowledge of the *Escherichia coli*  
 838      phosphoenolpyruvate-carbohydrate phosphotransferase system: Peculiarities of regulation and impact on  
 839      growth and product formation. *Applied Microbiology and Biotechnology*, 94(6):1483–1494.
- 840      Feist, A. M., Henry, C. S., Reed, J. L., Krummenacker, M., Joyce, A. R., Karp, P. D., Broadbelt, L. J., Hatzimanikatis,  
 841      V., and Palsson, B. Ø. (2007). A genome-scale metabolic reconstruction for *Escherichia coli* K-12 MG1655 that  
 842      accounts for 1260 ORFs and thermodynamic information. *Molecular Systems Biology*, 3(1):121.

- 844 Fernández-Coll, L., Maciąg-Dorszynska, M., Tailor, K., Vadia, S., Levin, P. A., Szalewska-Palasz, A., Cashel, M.,  
 845 and Dunny, G. M. (2020). The Absence of (p)ppGpp Renders Initiation of *Escherichia coli* Chromosomal DNA  
 846 Synthesis Independent of Growth Rates. *mBio*, 11(2):45.
- 847 Fijalkowska, I. J., Schaaper, R. M., and Jonczyk, P. (2012). DNA replication fidelity in *Escherichia coli*: A multi-DNA  
 848 polymerase affair. *FEMS Microbiology Reviews*, 36(6):1105–1121.
- 849 Finkelstein, I. J. and Greene, E. C. (2013). Molecular Traffic Jams on DNA. *Annual Review of Biophysics*, 42(1):241–  
 850 263.
- 851 Gama-Castro, S., Salgado, H., Santos-Zavaleta, A., Ledezma-Tejeida, D., Muñiz-Rascado, L., García-Sotelo, J. S.,  
 852 Alquicira-Hernández, K., Martínez-Flores, I., Pannier, L., Castro-Mondragón, J. A., Medina-Rivera, A., Solano-  
 853 Lira, H., Bonavides-Martínez, C., Pérez-Rueda, E., Alquicira-Hernández, S., Porrón-Sotelo, L., López-Fuentes,  
 854 A., Hernández-Koutoucheva, A., Moral-Chávez, V. D., Rinaldi, F., and Collado-Vides, J. (2016). RegulonDB  
 855 version 9.0: High-level integration of gene regulation, coexpression, motif clustering and beyond. *Nucleic  
 856 Acids Research*, 44(D1):D133–D143.
- 857 Ge, J., Yu, G., Ator, M. A., and Stubbe, J. (2003). Pre-Steady-State and Steady-State Kinetic Analysis of *E. coli* Class  
 858 I Ribonucleotide Reductase. *Biochemistry*, 42(34):10071–10083.
- 859 Godin, M., Delgado, F. F., Son, S., Grover, W. H., Bryan, A. K., Tzur, A., Jorgensen, P., Payer, K., Grossman, A. D.,  
 860 Kirschner, M. W., and Manalis, S. R. (2010). Using buoyant mass to measure the growth of single cells. *Nature  
 861 Methods*, 7(5):387–390.
- 862 Goldman, S. R., Nair, N. U., Wells, C. D., Nickels, B. E., and Hochschild, A. (2015). The primary  $\sigma$  factor in *Es-  
 863 cherichia coli* can access the transcription elongation complex from solution *in vivo*. *eLife*, 4:e10514.
- 864 Harris, L. K. and Theriot, J. A. (2018). Surface Area to Volume Ratio: A Natural Variable for Bacterial Morphogen-  
 865 esis. *Trends in microbiology*, 26(10):815–832.
- 866 Harris, R. M., Webb, D. C., Howitt, S. M., and Cox, G. B. (2001). Characterization of PitA and PitB from *Escherichia  
 867 coli*. *Journal of Bacteriology*, 183(17):5008–5014.
- 868 Heldal, M., Norland, S., and Tumyr, O. (1985). X-ray microanalytic method for measurement of dry matter and  
 869 elemental content of individual bacteria. *Applied and Environmental Microbiology*, 50(5):1251–1257.
- 870 Henkel, S. G., Beek, A. T., Steinsiek, S., Stagge, S., Bettenbrock, K., de Mattos, M. J. T., Sauter, T., Sawodny, O.,  
 871 and Ederer, M. (2014). Basic Regulatory Principles of *Escherichia coli*'s Electron Transport Chain for Varying  
 872 Oxygen Conditions. *PLoS ONE*, 9(9):e107640.
- 873 Ingledew, W. J. and Poole, R. K. (1984). The respiratory chains of *Escherichia coli*. *Microbiological Reviews*,  
 874 48(3):222–271.
- 875 Ireland, W. T., Beeler, S. M., Flores-Bautista, E., Belliveau, N. M., Sweredoski, M. J., Moradian, A., Kinney, J. B.,  
 876 and Phillips, R. (2020). Deciphering the regulatory genome of *Escherichia coli*, one hundred promoters at a  
 877 time. *bioRxiv*.
- 878 Jacob, F. and Monod, J. (1961). Genetic regulatory mechanisms in the synthesis of proteins. *Journal of Molecular  
 879 Biology*, 3(3):318–356.
- 880 Jensen, R. B., Wang, S. C., and Shapiro, L. (2001). A moving DNA replication factory in *Caulobacter crescentus*.  
 881 *The EMBO journal*, 20(17):4952–4963.
- 882 JL, R., S, V., D, S., ÁD, O., A, S., and M, H. (2016). Bacterial Persistence Is an Active  $\sigma$ S Stress Response to Metabolic  
 883 Flux Limitation. *Molecular Systems Biology*, 12(9):882.
- 884 Jun, S., Si, F., Pugatch, R., and Scott, M. (2018). Fundamental principles in bacterial physiology - history, recent  
 885 progress, and the future with focus on cell size control: A review. *Reports on Progress in Physics*, 81(5):056601.
- 886 Kapanidis, A. N., Margeat, E., Laurence, T. A., Doose, S., Ho, S. O., Mukhopadhyay, J., Kortkhonjia, E., Mekler, V.,  
 887 Ebright, R. H., and Weiss, S. (2005). Retention of Transcription Initiation Factor  $\Sigma$ 70 in Transcription Elonga-  
 888 tion: Single-Molecule Analysis. *Molecular Cell*, 20(3):347–356.
- 889 Khademi, S., O'Connell, J., Remis, J., Robles-Colmenares, Y., Miercke, L.J. W., and Stroud, R. M. (2004). Mechanism  
 890 of Ammonia Transport by Amt/MEP/Rh: Structure of AmtB at 1.35 Å. *Science*, 305(5690):1587–1594.

- 891 Khademian, M. and Imlay, J. A. (2017). *Escherichia coli* cytochrome c peroxidase is a respiratory oxidase that  
892 enables the use of hydrogen peroxide as a terminal electron acceptor. *Proceedings of the National Academy  
893 of Sciences*, 114(33):E6922–E6931.
- 894 Li, G.-W., Burkhardt, D., Gross, C., and Weissman, J. S. (2014). Quantifying absolute protein synthesis rates  
895 reveals principles underlying allocation of cellular resources. *Cell*, 157(3):624–635.
- 896 Liu, M., Durfee, T., Cabrera, J. E., Zhao, K., Jin, D. J., and Blattner, F. R. (2005). Global Transcriptional Programs  
897 Reveal a Carbon Source Foraging Strategy by *Escherichia coli*. *Journal of Biological Chemistry*, 280(16):15921–  
898 15927.
- 899 Lu, D., Grayson, P., and Schulten, K. (2003). Glycerol Conductance and Physical Asymmetry of the *Escherichia  
900 coli* Glycerol Facilitator GlpF. *Biophysical Journal*, 85(5):2977–2987.
- 901 Lynch, M. and Marinov, G. K. (2015). The bioenergetic costs of a gene. *Proceedings of the National Academy of  
902 Sciences*, 112(51):15690–15695.
- 903 Maaløe, O. (1979). *Regulation of the Protein-Synthesizing Machinery—Ribosomes, tRNA, Factors, and So On. Gene  
904 Expression*. Springer.
- 905 Milo, R., Jorgensen, P., Moran, U., Weber, G., and Springer, M. (2010). BioNumbers—the database of key num-  
906 bers in molecular and cell biology. *Nucleic Acids Research*, 38(suppl\_1):D750–D753.
- 907 Monod, J. (1947). The phenomenon of enzymatic adaptation and its bearings on problems of genetics and  
908 cellular differentiation. *Growth Symposium*, 9:223–289.
- 909 Mooney, R. A., Darst, S. A., and Landick, R. (2005). Sigma and RNA Polymerase: An On-Again, Off-Again Rela-  
910 tionship? *Molecular Cell*, 20(3):335–345.
- 911 Mooney, R. A. and Landick, R. (2003). Tethering  $\Sigma$ 70 to RNA polymerase reveals high *in vivo* activity of  $\sigma$  factors  
912 and  $\Sigma$ 70-dependent pausing at promoter-distal locations. *Genes & Development*, 17(22):2839–2851.
- 913 Neidhardt, F. C., Ingraham, J., and Schaechter, M. (1991). *Physiology of the Bacterial Cell - A Molecular Approach*,  
914 volume 1. Elsevier.
- 915 Ojkic, N., Serbanescu, D., and Banerjee, S. (2019). Surface-to-volume scaling and aspect ratio preservation in  
916 rod-shaped bacteria. *eLife*, 8:642.
- 917 Patrick, M., Dennis, P. P., Ehrenberg, M., and Bremer, H. (2015). Free RNA polymerase in *Escherichia coli*.  
918 *Biochimie*, 119:80–91.
- 919 Peebo, K., Valgepea, K., Maser, A., Nahku, R., Adamberg, K., and Vilu, R. (2015). Proteome reallocation in *Es-  
920 cherichia coli* with increasing specific growth rate. *Molecular BioSystems*, 11(4):1184–1193.
- 921 Perdue, S. A. and Roberts, J. W. (2011).  $\sigma^{70}$ -dependent Transcription Pausing in *Escherichia coli*. *Journal of  
922 Molecular Biology*, 412(5):782–792.
- 923 Phillips, R. (2018). Membranes by the Numbers. In *Physics of Biological Membranes*, pages 73–105. Springer,  
924 Cham, Cham.
- 925 Ramos, S. and Kaback, H. R. (1977). The relation between the electrochemical proton gradient and active trans-  
926 port in *Escherichia coli* membrane vesicles. *Biochemistry*, 16(5):854–859.
- 927 Rosenberg, H., Gerdes, R. G., and Chegwidden, K. (1977). Two systems for the uptake of phosphate in *Escherichia  
928 coli*. *Journal of Bacteriology*, 131(2):505–511.
- 929 Rudd, S. G., Valerie, N. C. K., and Helleday, T. (2016). Pathways controlling dNTP pools to maintain genome  
930 stability. *DNA Repair*, 44:193–204.
- 931 Sánchez-Romero, M. A., Molina, F., and Jiménez-Sánchez, A. (2011). Organization of ribonucleoside diphosphate  
932 reductase during multifork chromosome replication in *Escherichia coli*. *Microbiology*, 157(8):2220–2225.
- 933 Schaechter, M., Maaløe, O., and Kjeldgaard, N. O. (1958). Dependency on Medium and Temperature of Cell Size  
934 and Chemical Composition during Balanced Growth of *Salmonella typhimurium*. *Microbiology*, 19(3):592–606.
- 935 Schmidt, A., Kochanowski, K., Vedelaar, S., Ahrné, E., Volkmer, B., Callipo, L., Knoops, K., Bauer, M., Aebersold,  
936 R., and Heinemann, M. (2016). The quantitative and condition-dependent *Escherichia coli* proteome. *Nature  
937 Biotechnology*, 34(1):104–110.

- 938 Scholz, S. A., Diao, R., Wolfe, M. B., Fivenson, E. M., Lin, X. N., and Freddolino, P. L. (2019). High-Resolution  
 939 Mapping of the *Escherichia coli* Chromosome Reveals Positions of High and Low Transcription. *Cell Systems*,  
 940 8(3):212–225.e9.
- 941 Scott, M., Gunderson, C. W., Mateescu, E. M., Zhang, Z., and Hwa, T. (2010). Interdependence of cell growth and  
 942 gene expression: origins and consequences. *Science*, 330(6007):1099–1102.
- 943 Sekowska, A., Kung, H.-F., and Danchin, A. (2000). Sulfur Metabolism in *Escherichia coli* and Related Bacteria:  
 944 Facts and Fiction. *Journal of Molecular Microbiology and Biotechnology*, 2(2):34.
- 945 Shi, H., Bratton, B. P., Gitai, Z., and Huang, K. C. (2018). How to Build a Bacterial Cell: MreB as the Foreman of  
 946 *E. coli* Construction. *Cell*, 172(6):1294–1305.
- 947 Si, F., Le Treut, G., Sauls, J. T., Vadia, S., Levin, P. A., and Jun, S. (2019). Mechanistic Origin of Cell-Size Control  
 948 and Homeostasis in Bacteria. *Current Biology*, 29(11):1760–1770.e7.
- 949 Si, F., Li, D., Cox, S. E., Sauls, J. T., Azizi, O., Sou, C., Schwartz, A. B., Erickstad, M. J., Jun, Y., Li, X., and Jun, S. (2017).  
 950 Invariance of Initiation Mass and Predictability of Cell Size in *Escherichia coli*. *Current Biology*, 27(9):1278–1287.
- 951 Sirko, A., Zatyka, M., Sadowy, E., and Hulanicka, D. (1995). Sulfate and thiosulfate transport in *Escherichia coli* K-  
 952 12: Evidence for a functional overlapping of sulfate- and thiosulfate-binding proteins. *Journal of Bacteriology*,  
 953 177(14):4134–4136.
- 954 Stasi, R., Neves, H. I., and Spira, B. (2019). Phosphate uptake by the phosphonate transport system PhnCDE.  
 955 *BMC Microbiology*, 19.
- 956 Stevenson, B. S. and Schmidt, T. M. (2004). Life History Implications of rRNA Gene Copy Number in *Escherichia*  
 957 *coli*. *Applied and Environmental Microbiology*, 70(11):6670–6677.
- 958 Stouthamer, A. H. (1973). A theoretical study on the amount of ATP required for synthesis of microbial cell  
 959 material. *Antonie van Leeuwenhoek*, 39(1):545–565.
- 960 Stouthamer, A. H. and Bettenhaussen, C. W. (1977). A continuous culture study of an ATPase-negative mutant  
 961 of *Escherichia coli*. *Archives of Microbiology*, 113(3):185–189.
- 962 Svenningsen, S. L., Kongstad, M., Stenum, T. S. n., Muñoz-Gómez, A. J., and Sørensen, M. A. (2017). Transfer RNA  
 963 is highly unstable during early amino acid starvation in *Escherichia coli*. *Nucleic Acids Research*, 45(2):793–804.
- 964 Szenk, M., Dill, K. A., and de Graff, A. M. R. (2017). Why Do Fast-Growing Bacteria Enter Overflow Metabolism?  
 965 Testing the Membrane Real Estate Hypothesis. *Cell Systems*, 5(2):95–104.
- 966 Taheri-Araghi, S., Bradde, S., Sauls, J. T., Hill, N. S., Levin, P. A., Paulsson, J., Vergassola, M., and Jun, S. (2015).  
 967 Cell-size control and homeostasis in bacteria. - PubMed - NCBI. *Current Biology*, 25(3):385–391.
- 968 Tatusov, R. L., Galperin, M. Y., Natale, D. A., and Koonin, E. V. (2000). The COG database: a tool for genome-scale  
 969 analysis of protein functions and evolution. *Nucleic Acids Research*, 28(1):33–36.
- 970 Taymaz-Nikerel, H., Borujeni, A. E., Verheijen, P. J. T., Heijnen, J. J., and van Gulik, W. M. (2010).  
 971 Genome-derived minimal metabolic models for *Escherichia coli* mg1655 with estimated in vivo  
 972 respiratory ATP stoichiometry. *Biotechnology and Bioengineering*, 107(2):369–381. \_eprint:  
 973 <https://onlinelibrary.wiley.com/doi/pdf/10.1002/bit.22802>.
- 974 The Gene Ontology Consortium (2018). The Gene Ontology Resource: 20 years and still GOing strong. *Nucleic  
 975 Acids Research*, 47(D1):D330–D338.
- 976 Valgepea, K., Adamberg, K., Seiman, A., and Vilu, R. (2013). *Escherichia coli* achieves faster growth by increasing  
 977 catalytic and translation rates of proteins. *Molecular BioSystems*, 9(9):2344.
- 978 van Heeswijk, W. C., Westerhoff, H. V., and Boogerd, F. C. (2013). Nitrogen Assimilation in *Escherichia coli*: Putting  
 979 Molecular Data into a Systems Perspective. *Microbiology and Molecular Biology Reviews*, 77(4):628–695.
- 980 Weber, J. and Senior, A. E. (2003). ATP synthesis driven by proton transport in F1FO-ATP synthase. *FEBS Letters*,  
 981 545(1):61–70.
- 982 Willsky, G. R., Bennett, R. L., and Malamy, M. H. (1973). Inorganic Phosphate Transport in *Escherichia coli*: Involvement  
 983 of Two Genes Which Play a Role in Alkaline Phosphatase Regulation. *Journal of Bacteriology*, 113(2):529–  
 984 539.

- 985 Zhang, L., Jiang, W., Nan, J., Almqvist, J., and Huang, Y. (2014a). The *Escherichia coli* CysZ is a pH dependent sulfate  
986 transporter that can be inhibited by sulfite. *Biochimica et Biophysica Acta (BBA) - Biomembranes*, 1838(7):1809–  
987 1816.
- 988 Zhang, Z., Aboulwafa, M., and Saier, M. H. (2014b). Regulation of crp gene expression by the catabolite repres-  
989 sor/activator, cra, in *Escherichia coli*. *Journal of Molecular Microbiology and Biotechnology*, 24(3):135–141.
- 990 Zhu, M. and Dai, X. (2019). Growth suppression by altered (p)ppGpp levels results from non-optimal resource  
991 allocation in *Escherichia coli*. *Nucleic Acids Research*, 47(9):4684–4693.